Biomedicine & Pharmacotherapy 180 (2024) 117523

Contents lists available at ScienceDirect

Biomedicine & Pharmacotherapy

journal homepage: www.elsevier.com/locate/biopha

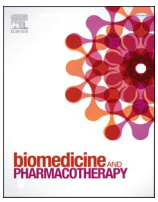

Polypharmacological profiling across protein target families and cellular pathways using the multiplexed cell-based assay platform safetyProfiler reveals efficacy, potency and side effects of drugs

Lukša Popović [a,b], Ben Brankatschk [b], Giulia Palladino [a,b], Moritz J. Rossner [c], Michael C. Wehr [a,b,*]

[a] Research Group Cell Signalling, Department of Psychiatry and Psychotherapy, LMU University Hospital, LMU Munich, Nussbaumstr. 7, Munich 80336, Germany
[b] Systasy Bioscience GmbH, Fraunhoferstr. 8, Planegg-Martinsried 82152, Germany
[c] Section of Molecular Neurobiology, Department of Psychiatry and Psychotherapy, LMU University Hospital, LMU Munich, Nussbaumstr. 7, Munich 80336, Germany

ARTICLE INFO

Keywords:
Drug development
Early drug discovery
Attrition rates
Safety profiling
Side effects
Drug efficacy
Drug toxicity
Molecular barcoding
Disease-relevant drug targets
Nuclear receptors
G protein coupled receptors
Receptor tyrosine kinases
EGFR
Tyrosine kinase inhibitors
Compound profiling
Cell-based assay
Barcoded assay
Multiparametric assay
Multiplex assay
Split TEV assay

ABSTRACT

Selectivity profiling is key for assessing the pharmacological properties of multi-target drugs. We have developed a cell-based and barcoded assay encompassing ten druggable targets, including G protein-coupled receptors (GPCRs), receptor tyrosine kinases (RTKs), nuclear receptors, a protease as well as their key downstream pathways and profiled 17 drugs in living cells for efficacy, potency, and side effects. Notably, this multiplex assay, termed safetyProfiler assay, enabled the simultaneous assessment of multiple target and pathway activities, shedding light on the polypharmacological profile of compounds. For example, the neuroleptics clozapine, paliperidone, and risperidone potently inhibited primary targets DRD2 and HTR2A as well as cAMP and calcium pathways. However, while paliperidone and risperidone also potently inhibited the secondary target ADRA1A and mitogen-activated protein kinase (MAPK) downstream pathways, clozapine only exhibited mild antagonistic effects on ADRA1A and lacked MAPK inhibition downstream of DRD2 and HTR2A. Furthermore, we present data on the selectivity for bazedoxifene, an estrogen receptor antagonist currently undergoing clinical phase 2 trials for breast cancer, on MAPK signaling. Additionally, precise potency data for LY2452473, an androgen receptor antagonist, that completed a phase 2 clinical trial for prostate cancer, are presented. The non-selective kinase inhibitor staurosporine was observed to potently inactivate the two RTKs EGFR and ERBB4 as well as MAPK signaling, while eliciting stress-related cAMP responses. Our findings underscore the value of comprehensive profiling in elucidating the pharmacological properties of established and novel therapeutics, thereby facilitating the development of novel multi-target drugs with enhanced efficacy and selectivity.

1. Introduction

Drug development is a long and costly process, easily consuming more than 10 billion USD per drug within a time frame of 15 years or more. In addition, drug development suffers from high attrition rates that become most relevant in the clinical stages where a discontinued drug causes high financial losses [1,2]. Drugs that are approved by the United States Food and Drug Association (FDA) or European Medicines Agency (EMA) and have reached the market may also be withdrawn or discontinued from production in about 10 % of the cases (308 withdrawn/3445 approved, as of 13 August 2024 inquired at the CheMBL database (https://www.ebi.ac.uk/chembl/visualise/)), adding another twist to attrition [3]. The primary reasons for the discontinuation of a drug are typically safety-related, such as the occurrence of hepatotoxicity, the abuse of the drug, or a lack of efficacy [4–6]. Attrition occurs when drugs are promiscuous, i.e., when they have detrimental off-target effects, and side-effects are too severe [7,8]. Therefore, understanding the modulatory effects exerted by a drug candidate on disease-relevant targets and physiological pathways is crucial to develop better drugs. An assessment of compound effects is particularly

* Corresponding author at: Research Group Cell Signalling, Department of Psychiatry and Psychotherapy, LMU University Hospital, LMU Munich, Nussbaumstr. 7, Munich 80336, Germany.
E-mail address: michael.wehr@med.uni-muenchen.de (M.C. Wehr).

https://doi.org/10.1016/j.biopha.2024.117523
Received 16 August 2024; Received in revised form 1 October 2024; Accepted 4 October 2024
Available online 14 October 2024

important for multi-target drugs that are designed to treat complex diseases, such as cancer and neurological disorders [9,10].

To advance drug discovery and to reduce attrition, four leading pharmaceutical companies (Pfizer, Novartis, GlaxoSmithKline, and AstraZeneca) proposed to test whether drugs at the early stage of drug discovery exhibit off-target effects already *in cellulo* [10–13]. Such an early-on control screening of drug candidates is expected to facilitate a better understanding of a compound's pharmacological profile by assessing a compound's affinity to the desired targets vs. off-targets and by understanding which pathways vs. off-pathway effects (i.e., toxicity) are modulated by a compound. As a result, compounds with an appropriate pharmacological profile may progress faster to preclinical tests and possibly clinical trials, with an increased likelihood of reducing attrition and advancing to approval. The aforementioned four companies compiled a list of the most prevalent drug targets to be subjected to screening for severe side effects: G protein-coupled receptors (GPCRs), enzymes (e.g., kinases, in particular receptor tyrosine kinases (RTKs), proteases, esterases), nuclear receptors, epigenetic modifiers, ion channels, and transporters [13,14]. The development of multiplex assays allowed the acquisition of multiple independent readouts from the same sample. When using molecular barcodes, i.e., short stretches of nucleotides (DNA or RNA) as reporters for measuring cellular signaling events, the multiplexing capacity is only limited by the robust sequencing of the barcodes using next-generation sequencing (NGS) [15–17]. Barcoded reporter assays have been described for single protein families, such as GPCRs, for which the activity was measured through β-arrestin recruitment assays, either based on split TEV protease (TEVp) [18] or full TEVp [19] approaches, or a cAMP responsive pathway assay [20]. In addition, we have reported the barcoded profiling for ERBB receptors, an RTK subfamily [21]. Simultaneously assessing the activity of various drug target families, including their effects on central downstream pathways, is expected to improve both on-target and on-pathway selectivity [13,22–24]. Here, we describe the development of a multiparametric assay platform, termed safetyProfiler, to simultaneously profile efficacy and side effects of compounds on targets from different protein classes and physiological pathways in living cells. We integrate disease-relevant drug target classes of GPCRs, RTKs, nuclear receptors, and proteases into one multiplexed cell-based assay using molecular barcodes as readout. Lastly, we demonstrate the use of the safetyProfiler assay by profiling approved neuroleptics, antineoplastics that were recently approved or are in the later stages of clinical trials, and compound candidates that failed in development programs.

2. Materials & methods

2.1. Plasmids

Open reading frames (ORFs) of nuclear receptors (androgen receptor, (AR), estrogen receptor 1 (ESR1), glucocorticoid receptor (GR, NR3C1)) were purchased from Plasmid ID Harvard (murine Ar, MmCD00321218) or the plasmid repository DNASU (human ESR1, HsCD00000871; human GR, HsCD00651869) and then PCR amplified using Pwo polymerase (Sigma-Aldrich, 03789403001). PCR products were recombined into the pDONR/Zeo vector and sequence-verified to yield entry vectors for Gateway recombination cloning. Ar, ESR1, and GR entry vectors were then recombined into a GAL4-DNA binding domain (GAL4-DBD) containing Gateway destination vector (pBK_GAL4-DBD) to yield GAL4-DBD-Ar, GAL4-DBD-ESR1, and GAL4-DBD-GR fusions. Other plasmids were previously described, specifically split TEV assay vectors for GPCRs (adrenoreceptor alpha 1A (ADRA1A), vasopressin receptor 1A (AVPR1A), dopamine receptor D2 (DRD2), serotonin receptor 2A (HTR2A), the split TEV assay GPCR adapter β-arrestin-2 (ARRB2) fused to the C-terminal fragment of TEVp (ARRB2–1–383-CTEV) [18] and RTKs (epidermal growth factor receptor (EGFR), Erb-B2 Receptor Tyrosine Kinase 4 (ERBB4)) [21]. For these GPCR and RTK targets, ORFs were fused to the N-terminal fragment of TEVp (NTEV), a TEVp cleavage site (tcs) and the artificial transcriptional co-activator GAL4-VP16 (GV) to yield GPCR-/RTK-NTEV-tcs-GV plasmids. Likewise, the plasmids encoding the GPCR split TEV assay adapter β-arrestin-2 (ARRB2) fused to the C-terminal fragment of the TEVp (CTEV) to yield ARRB2–1–383-CTEV [18], the synthetic RTK split TEV assay adapter 3xSH2(GRB2) fused to CTEV to yield 3xSH2 (GRB2)-CTEV-2xHA [21], β-secretase 1 (BACE1) and its substrate Neuregulin-1 fused to GV to yield Nrg1-GV [25], as well as barcoded reporter constructs with 10x clustered upstream activating sequences (10xUAS), 6x clustered cAMP responsive elements (CRE), endogenous promoter region of the human EGR1 gene (EGR1p), 6x clustered nuclear factor of activated T-cells response elements (NFAT-RE) [26], and 12x clustered GR response elements (GR-RE) [27] were described before. In addition, barcoded reporters for AR (8x clustered AR response elements, AR-RE) and ESR1 (12x clustered ESR1 response elements, ER-RE) were cloned. The general structure of these plasmids is shown in Fig. S1. All plasmids used in this study can be found in Table S1. Plasmids are available from Addgene.

2.2. Chemical reagents

The following commercial compounds were used in this study: epinephrine (Sigma-Aldrich, E4642), vasopressin (Sigma-Aldrich, V9879), dopamine hydrochloride (Sigma-Aldrich, H8502), serotonin hydrochloride (Tocris, 3547), EGF (Sigma-Aldrich, E9644), EGFld (Sigma-Aldrich, H7660), norgestrel (Cayman Chemical, 10006319), β-estradiol (Sigma-Aldrich, E2758), dexamethasone (Sigma-Aldrich, D4902), AG1478 (Selleckchem, S2728), BACE1 inhibitor IV (Cayman Chemical, 23388), bazedoxifene (Sigma-Aldrich, PZ0018), canrenone (Santa Cruz, sc-205616), clozapine (Sigma-Aldrich, C6305), DAPT (Enzo Life Sciences, AXL-270–416-M005), elacestrant (MedChemExpress, HY-19822), LE300 (MedChemExpress, HY-103428), LY2452473 (MedChemExpress, HY-114530), mifepristone (Sigma-Aldrich, M8046), nocodazole (Sigma-Aldrich, M1404), paliperidone (Sigma-Aldrich, P0099), pyrotinib (MedChemExpress, HY-104065), relacorilant (Selleckchem, E1091), risperidone (Sigma-Aldrich, R3030), spironolactone (Selleckchem, S4054), staurosporine (MedChemExpress, HY-15141), tricine (Sigma-Aldrich, T-0377), $(MgCO_3)_4$ * $Mg(OH)_2$ * $5H_2O$ (Sigma-Aldrich, M5671), $MgSO_4$ * $7H_2O$ (Ecogen, A6287), EDTA (Thermo Fisher Scientific, 15575), DTT (Thermo Fisher Scientific, R0862), coenzyme A (PJK, 102212), D-luciferin (PKJ, 102112), ATP (PJK, 102261).

2.3. Cell culture

HEK293 (ATCC, CRL-1573), PC12 (Clontech, 631134), T-47D (ATCC, HTB133) and U2OS (HTB96) cell lines were cultured at 37 °C with 5 % CO_2 until reaching 80–90 % confluency before being split 1:5 or 1:10 for maintenance. Cells were kept in culture until passage 20. HEK293 cells were cultured in DMEM containing 4.5 g/L glucose (Thermo Fisher Scientific, 21969035), supplemented with 10 % FBS (Thermo Fisher Scientific, A5256801). PC12 cells were grown in DMEM with 1 g/L glucose (Thermo Fisher Scientific, 11880028), supplemented with 10 % FBS and 5 % horse serum (Thermo Fisher Scientific, 16050122). T-47D cells were maintained in RPMI 1640 (Thermo Fisher Scientific, 61870036) containing 500 μg/L h-Insulin (Sigma-Aldrich, I9278) and 10 % FBS. U2OS cells were maintained in McCoy's 5A medium (Thermo Fisher Scientific, 36600088) supplemented with 10 % FBS. All maintenance media were supplemented with 2 mM GlutaMAX (Thermo Fisher Scientific, 35050038) and 100 U/mL Penicillin/Streptomycin (Thermo Fisher Scientific, 15140122). For PC12 cells, all surfaces were coated with poly-L-lysine (0.02 M) for both maintenance and experiments. The transfection media for all four cell lines were formulated analogously to the maintenance media, with the exclusion of penicillin/streptomycin antibiotics. Starvation media for all cell lines

were supplemented with 1 % dialyzed FBS, except for U2OS cells, where 1 % regular non-dialyzed FBS was used. Cell-based assays were performed in starvation conditions.

2.4. Luciferase reporter assays

Cells were seeded into a white 96-well plate (20,000 cells/well for HEK293, T-47D, and U2OS cells; 50,000 cells/well for PC12 cells) and incubated for 24 h. On the following day, cells were transfected using lipofectamine 3000. Specifically, plasmid DNA was mixed with P3000 in a 1 μg:2 μL ratio and diluted in OptiMEM. In a second tube, LF3000 was diluted in OptiMEM in a 1 μg:3 μL ratio. The LF3000/OptiMEM mixture was shortly vortexed and left 5 mins at the room temperature prior to mixing it with the DNA/P3000 mixture, vortexed, and incubated at room temperature for 20 minutes. As reference, in assays using only a reporter plasmid (e.g., nuclear receptor response element, CRE element), 30 ng per plasmid were transfected per well. In assays using a plasmid encoding a nuclear receptor and a reporter plasmid, 15 ng of each plasmid were transfected per well. In GPCR, RTK, and BACE1 assays, 10 ng of each a plasmid encoding the target, a plasmid encoding the adapter or protease reporter, and a reporter plasmid were transfected per well. The pipetting scheme for all luciferase reporter assays with fixed endpoints of treatment is provided in Table S2. 30 μL of the transfection mixture was added to each well of a 96-well plate well and incubated for 2 h at 37 °C in 5 % CO_2, followed by the addition of 70 μL of transfection media per well and left for another 22 h at 37 °C with 5 %

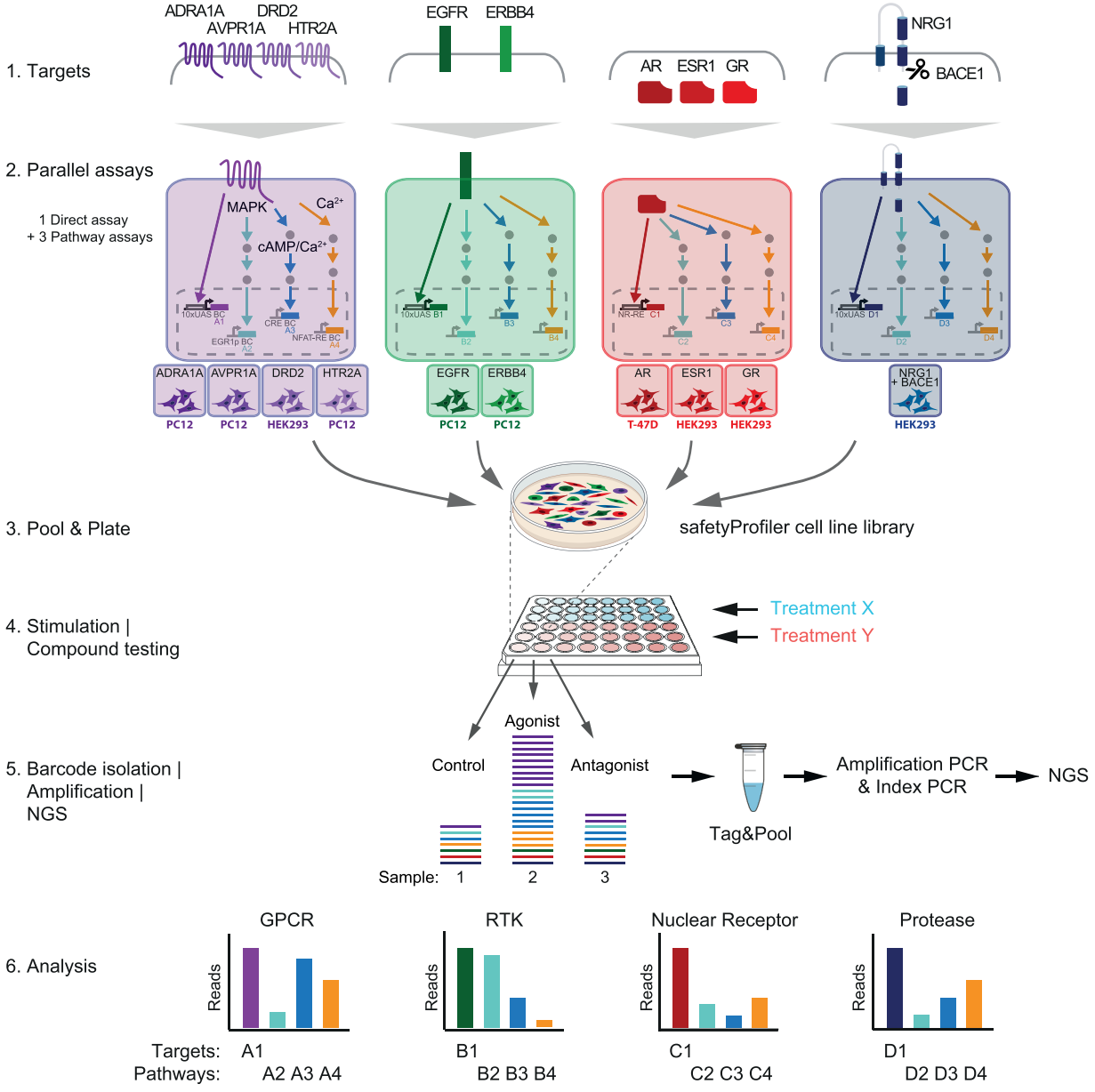

Fig. 1. Concept of the safetyProfiler assay, a comprehensive and multiplexed assay to simultaneously measure activities of multiple protein families and key downstream signaling pathways. Assays for G protein coupled receptors (GPCRs), receptor tyrosine kinases (RTKs), nuclear receptors, and the protease BACE1 were conducted in HEK293, PC12, and T-47D cell lines using synthetic barcode reporters for direct activity assays (split TEV assays for GPCRs and RTKs, translocation assays for nuclear receptors on their response elements (RE), and a BACE1 cleavage assay) and pathways (EGR1p for MAPK/ERK signaling, CRE for cAMP/calcium signaling, and NFAT-RE for pure calcium signaling). Assay cells are pooled and plated into 48-well plates, where the compounds are tested. Following the cell lysis, barcodes are extracted, PCR-amplified and sequenced. Sequencing results are analysed and visualized. 10xUAS, 10x clustered upstream activating sequences; BC, barcode.

CO_2. Cells were then serum starved for 24 hours, followed by compound treatment. Dose-response assays were conducted at the peak times of stimulation (c.f. Fig. 2 and S2), while profiler optimization and validation assays were stimulated for 12 h before lysing cells with 30 µL Passive Lysis Buffer (PLB) per well. Plates with cellular lysates were treated for 10 mins at 300 rpm to guarantee complete lysis. For measurement, 50 µl of a luciferase substrate buffer (20 mM tricine, 1.07 mM $(MgCO_3)_4$ * $Mg(OH)_2$ * $5H_2O$, 2.67 mM $MgSO_4$ * $7H_2O$, 100 µM EDTA, 33.3 µM DTT, 270 µM coenzym A, 530 µM ATP, 470 µM D-luciferin) were added. Luciferase activity was measured with Mithras LB 940381 Microplate Reader (Berthold Technologies) and analyzed using the software MicroWin2000.

2.5. Live cell luciferase assays

To determine the optimal timing for safetyProfiler assays, either 800,000 PC12 cells, or 500,000 HEK293 or T-47D cells were seeded onto a 3.5 cm dish. The protocol outlined in the luciferase reporter assays section was followed with one modification as 300 ng per plasmid was used. Split TEV assays for monitoring the activity of GPCRs and RTKs included plasmids for GPCR/RTK-NTEV-tcs-GV and ARRB2–1–383-CTEV (for GPCR split TEV assays, Addgene plasmid 194382) and GRB2 (SH2)-CTEV (for RTK split TEV assays, Addgene plasmid 214614), as well as the pGL4–10xUAS-MLPmin-luc2 reporter plasmid (Addgene plasmid 194383). Nuclear receptor assays used a plasmid expressing the nuclear receptor, a blank plasmid for normalizing plasmid amount, and the 10xUAS-MLPmin-luc2 reporter plasmid. The protease assay consisted of the BACE1 plasmid, the Nrg1-GV substrate plasmid, and the 10xUAS-MLPmin-luc2 reporter plasmid. Two replicates were run per condition. Post transfection, 0.1 % D-luciferin (Promega) was added to the cell culture medium. The dishes were then placed into a Lumicycle 32 device (ActiMetrics), which was placed inside an incubator set to 37 °C and 5 % CO_2 to monitor luminescence. For analysis, readings from the first time point after adding a stimulus were subtracted from all subsequent time points, and the replicates were averaged along with their standard deviations. Since the BACE1/ Nrg1-GV assay was a constitutive assay, cells were cultured for 4 h inside an incubator, before the transfection medium was replaced with the starvation medium. Next, dishes were placed into the Lumicycle 32 and luminescence was continuously recorded. The 3.5-cm dishes were always wrapped in Parafilm to minimize evaporation. The resulting data were visualized using Excel line charts.

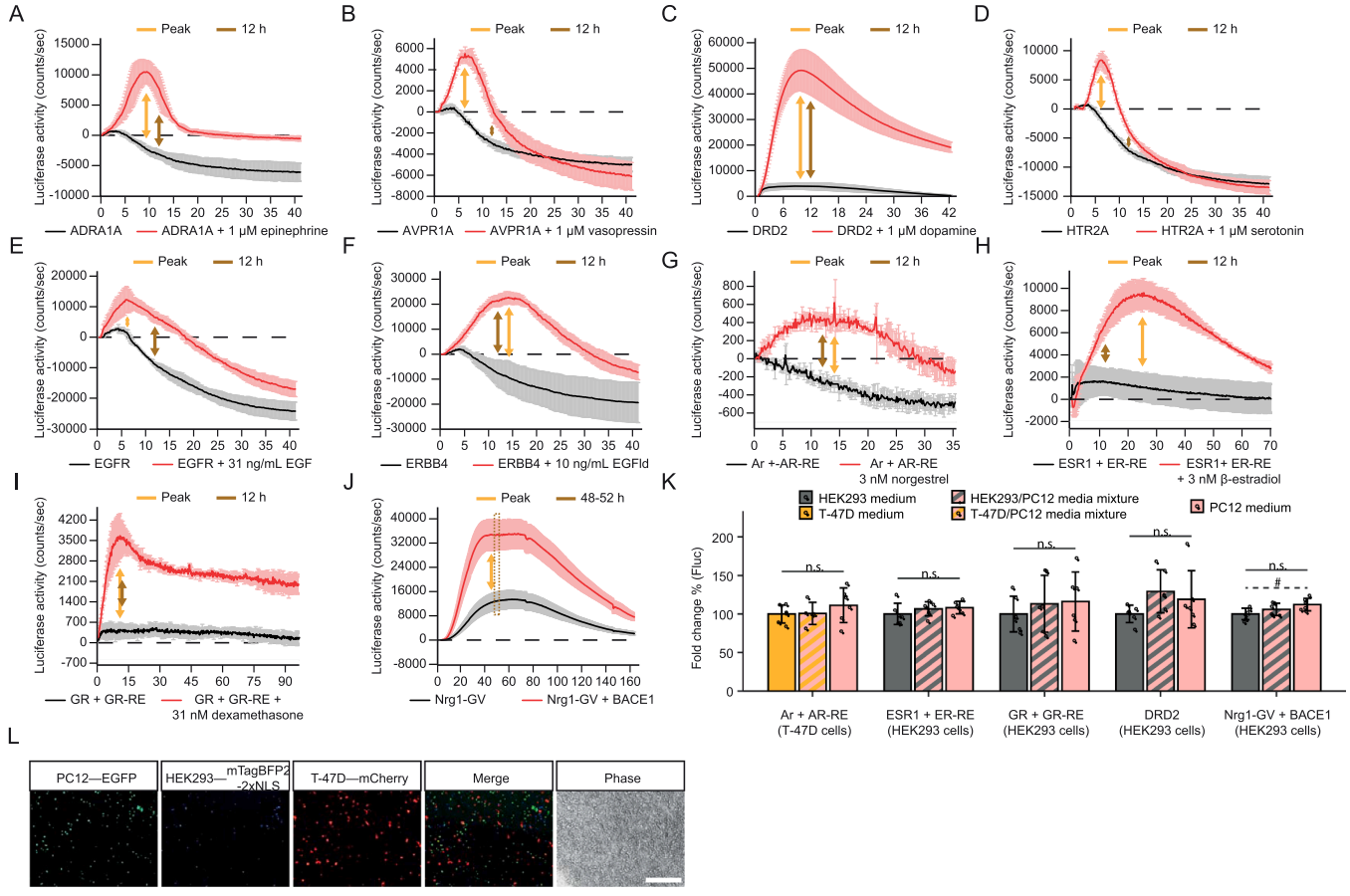

Fig. 2. Single target assays exhibit an overlapping measurement window of twelve hours after treatment. (A-I) Live cell luciferase assays of single receptor assays included in the safetyProfiler upon stimulation with their respective ligands. Arrows in light yellow indicate the time point with peak activity, arrows in dark yellow indicate the response 12 h after the stimulation (for A-I) or dashed box in dark yellow indicates 48–52 h after transfection (for J). Light red and light gray area represent SD, n = 2. (A) ADRA1A in PC12 cells. (B) AVPR1A in PC12 cells. (C) DRD2 in HEK293 cells. (D) HTR2A in PC12 cells. (E) EGFR in PC12 cells. (F) ERBB4 in PC12 cells. (G) Ar in T-47D cells. (H) ESR1 in HEK293 cells. (I) GR in HEK293 cells. GPCR and RTK assays were conducted with the split TEV technique and a 10xUAS luciferase reporter as readout. Nuclear receptors assays were performed with their respective response elements as readout. (J) Live cell luciferase assay of constitutive BACE1 activity using Nrg1-GV as substrate in HEK293 cells. An assay without transfected BACE1 was used as control. (K) PC12 medium does not affect assays developed in HEK293 and T-47D cells. Depicted are fold changes of Ar, ESR1, GR, and DRD2 upon stimulation with their respective ligands as well as the fold change of BACE1-mediated cleavage of Nrg1-GV in regular medium (i.e., HEK293 or T-47D medium), 50:50 mixture of regular medium and PC12 medium, and PC12 medium only. The fold change in the regular medium was set to 100 %. Error bars represent SD, n = 6. Significance was calculated using 1way ANOVA with Benjamini-Hochberg post-hoc test. n.s., non-significant; $p < 0.1$, #. (L) PC12, HEK293, and T-47D cell exhibit regular morphology when co-cultured for 48 hours in PC12 medium. Cells were transiently transfected with fluorescent proteins as shown above images. Scale bar is 500 µm.

2.6. Fluorescence microscopy

800,000 PC12, 500,000 HEK293, and 500,000 T-47D cells were seeded in separate wells of a 6-well plate at 37 °C with 5 % CO_2 followed by the transfection with 600 ng of vectors encoding fluorescent proteins (pEGFP-C1, pMK1344-mTagBFP2–2xNLS, pCherry-C2, for the three cell lines, respectively) using lipofectamine 3000. Next day, cells were trypsinized and co-cultured on a poly-L-lysine (0.02 M) coated surface in DMEM (1 g/L glucose) with 10 % FBS, 5 % horse serum, 2 mM GlutaMAX, and 100 U/mL penicillin/streptomycin media. Cells were seeded in a manner that each cell line covers the equal amount of a dish/well surface (33.33 % in case of three cell lines, or 50 % in case of two cell lines). On day two, cells were serum-starved in 1 % dialyzed FBS and imaged daily for 96 h on a ZEISS Axio Observer.Z1 microscope with a C-Apochromat 63/1.20 W Corr objective.

2.7. Barcoded multiplex assays

The experiment was performed following the published protocol for barcoded profiler assays [28], with a few adjustments using three cell lines and different well formats. First, the number of cells required per assay was calculated based on the number of conditions and the well size. The percentage of each cell line required per well was calculated based on the percentage of assays conducted in the respective cell line to assess the surface area per well covered by each cell line (e.g., 6/13 assays in PC12 cells, 46.1 % surface area; 5/13 assays in HEK293 cells, 38.5 % surface area; 2/13 assays in T-47D cells, 15.4 % surface area), to maintain consistency across batches, and to simplify the calculation for the transfection process. Taken together, this approach ensures a comparable distribution of barcode reporters across batches and wells, preventing overrepresentation or underrepresentation of specific barcodes. The reader is advised to note that 13 assays consisted of 10 target assays and 3 control assays. Therefore, for assays in the 12-well plate format, 150,000 HEK293 cells, 150,000 T-47D cells, and 450,000 PC12 cells were required per well, calculating for a single cell line per well. For the 48-well plate format, cell numbers were reduced to 35,000 HEK293 cells, 35,000 T-47D cells, and 112,500 PC12 cells per well, also calculating cell numbers for a single cell line per well. Plasmids were transfected into 13 batches of cells using in-solution transfection. Table S3 summarizes all combinations of barcoded assays conducted, whereas Table S1 contains the sequences of barcodes used as RNA reporters. Specifically, cells were kept in the in-solution transfection mixture for 2 h at 37 °C with 5 % CO_2. The Falcon tube was slightly tilted, with the lid slightly unscrewed to allow better atmosphere flow. Cells were then centrifugated at 1000 rpm for 5 min, the transfection media was aspirated, and the cells were resuspended in 2 mL

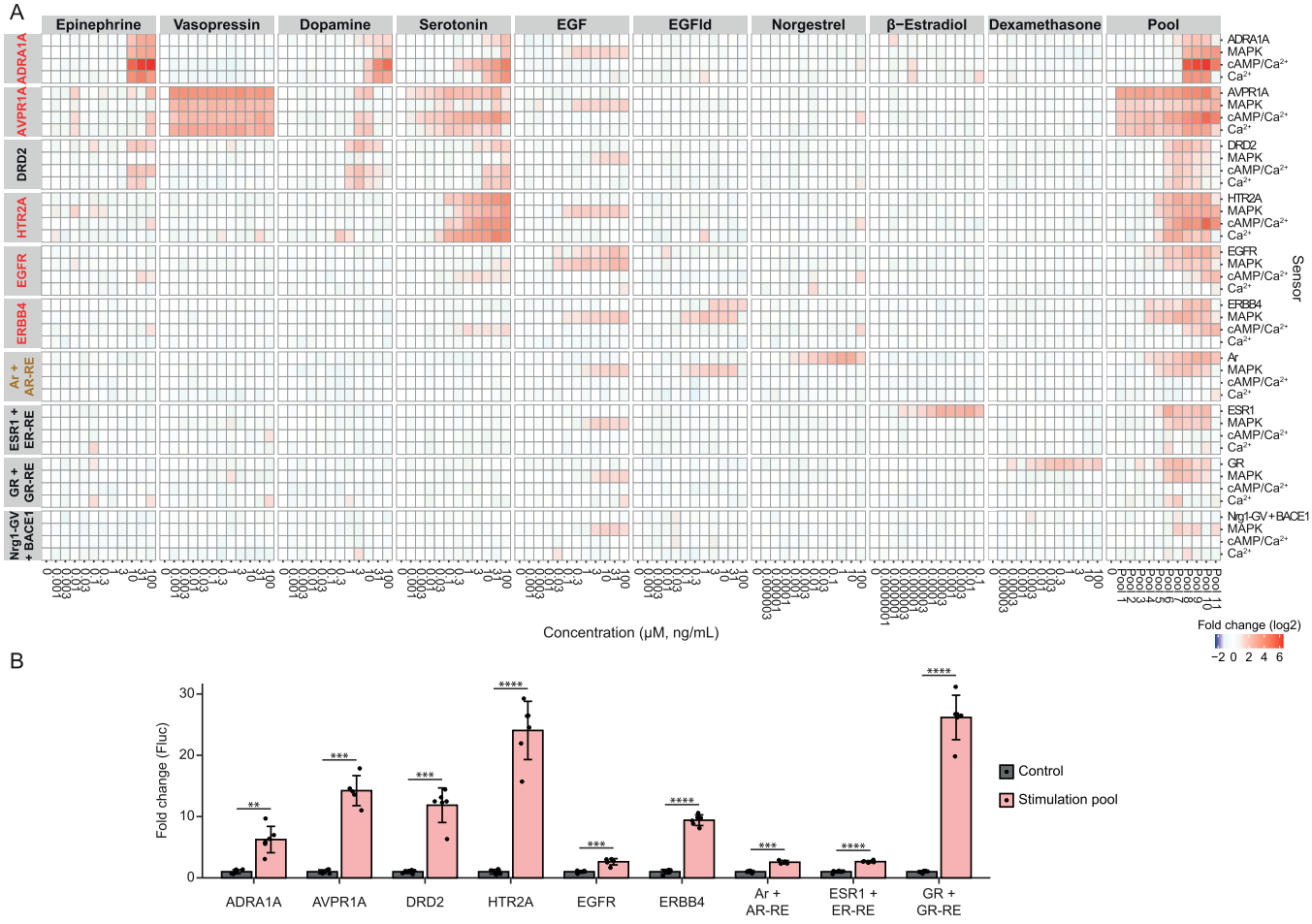

Fig. 3. The pooling of stimuli enables the simultaneous and robust activation of target assays. (A) Heatmap showing stimulation profiles on GPCRs, RTKs, nuclear receptors, and their downstream signaling pathways. GPCR and RTK activities were measured using split TEV assays and barcoded UAS reporters. Activities of nuclear receptors and signaling pathways were measured with barcoded reporters containing response elements and promoters. BACE1 activity was measured using the cleavage of the synthetic substrate Nrg1-GV and the concomitant activation of a barcoded UAS reporter. Compound effects are shown as log2-transformed fold change. (B) Pooled stimuli (1 μM epinephrine, 1 μM vasopressin, 1 μM dopamine, 1 μM serotonin, 31.6 ng/mL EGF, 10 ng/mL EGFld, 2 nM norgestrel, 1 nM β-estradiol, 31.6 nM dexamethasone) activated single assays without toxicity. Bar graphs show fold change 12 h post stimulation. Control assays were normalized to 1. Error bars represent SD, n = 5. Significance was measured using student's t-test. $p < 0.01$, **; $p < 0.001$, ***; $p < 0.0001$, ****.

maintenance medium per assay. Resuspended cells were transferred to a 250 mL flask (Sarstedt, 83.1822.003) and the rest of the maintenance media was added prior to thorough mixing of the bottle to have transfected cells equally distributed. Cells were then either seeded into a 12-well plate (stimulation assay, Fig. 3) with 58,000 HEK293 cells (calculated as 150,000 cells * 5/13 assays), 23,000 T-47D cells (calculated as 150,000 cells * 2/13 assays), and 208,000 PC12 cells (calculated as 450,000 cells * 6/13 assays) per well, or into a 48-well plate (antagonist assay, Fig. 4) with 13,500 HEK293 cells (calculated as 35,000 cells * 5/13 assays), 5500 T-47D cells (calculated as 35,000 cells * 2/13 assays), and 52,000 PC12 cells (calculated as 112,500 cells * 6/13 assays) per well for 24 h. On the following day, the medium was replaced with serum starvation medium (1 % dialysed FBS), followed by 12 h compound treatments. Cells were then lysed by adding 1300 µL (12-well plate) or 325 µL (48-well plate) Tag&Pool lysis buffer (100 mM Tris/HCl pH 7.5, 500 mM LiCl, 10 mM EDTA, 5 mM DTT, 1 % LiDS).

2.8. Tag&Pool procedure for the combined processing of samples

In the Tag&Pool procedure, 24 cell lysates are combined for single-step purification and processing of barcode reporter RNAs. Secondary barcodes were added to the lysates at 0.125 µM for annealing at 65 °C for 15 min to track individual wells. After cooling to room temperature, lysates from a 12-well plate were pooled with 20 µL of M-PVA OdT2 beads (Chemagen, Cat. No. CMG-231), while lysates from a 48-well plate were pooled with 10 µL of M-PVA OdT2 beads. Beads underwent five washes, including one with 100 µL of 1x High-Capacity reaction buffer (High-Capacity cDNA Reverse Transcription Kit, Thermo Fisher Scientific, Cat. No. 4368814). cDNA synthesis was then performed on the beads in 20 µL of High-Capacity cDNA Reverse Transcription mix at 25 °C for 25 min. Barcoded cDNA was amplified using a forward primer with the Read1 Illumina adapter and a unique molecular identifier (UMI), and a Read2 reverse primer for 30 PCR cycles. Illumina indices and sequencing adapters were added in an additional 10 PCR cycles. The barcode libraries were pooled equimolarly (2 pM) and sequenced using paired-end, dual-index sequencing with the NovaSeq 6000 SP Reagent Kit v1.5 (Illumina GmbH, Cat. No. 20028401 or 20040719). Oligonucleotides used are listed in Table S4.

2.9. Toxicity assay

Elacestrant toxicity was evaluated using the CCK-8 kit (Gerbu Biotechnik GmbH) according to the manufacturer's instructions. Cells were seeded in clear-bottom 96-well plates and treated according to the instructions in the section on luciferase reporter assays. Increasing concentrations of elacestrant were applied to the cells, along with 10 µL/well of the CCK-8 solution, and the plates were incubated at 37 °C with 5 % CO_2 for 12 h in the dark. Cell viability was assessed by measuring absorbance at 450 nm using an Epoch Microplate Spectrometer (BioTek Instruments). The absorbance values were normalized to the untreated control, set as 1.

2.10. Quantification and statistical analysis

2.10.1. Data analysis

For barcode reporter assays, sequencing reads from each transfected

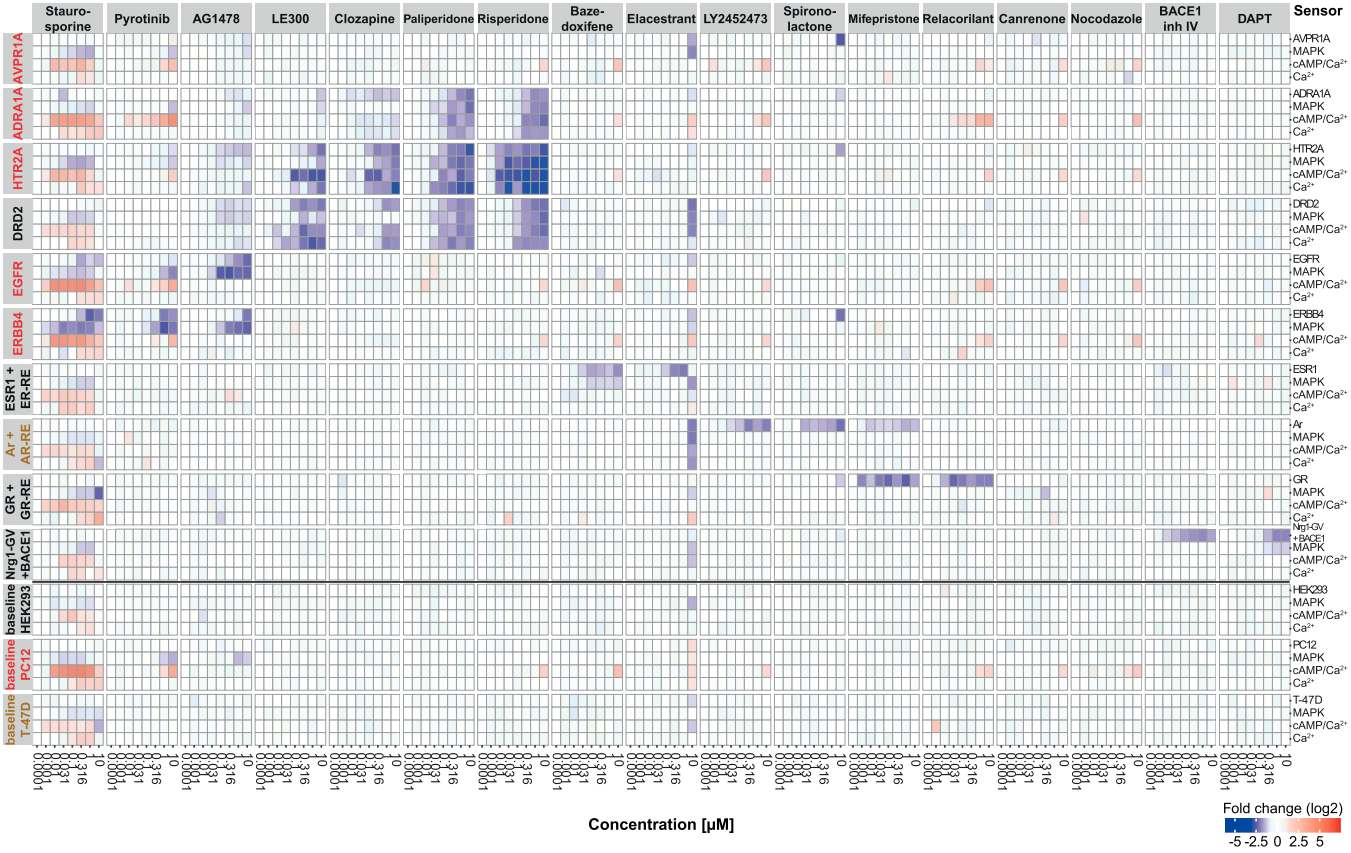

Fig. 4. The barcoded safetyProfiler assay reveals selectivity properties of antineoplastics, neuroleptics and failed drugs on targets and pathways. Heatmap showing antagonistic effects of compounds on GPCRs, RTKs, nuclear receptors, BACE1 and downstream signaling pathways. Depending on the target, the assay was conducted in PC12 cells (red font), HEK293 cells (black font), and T-47D cells (brown font). Principles of assays for GPCRs, RTKs, nuclear receptors, BACE1, and signaling pathways were as described in Fig. 3A. In addition to the increasing concentrations of the compounds shown, all assays contained constant concentrations of epinephrine (1 µM), vasopressin (1 µM), dopamine (1 µM), serotonin (1 µM), EGF (31.6 ng/mL), EGF-like domain (10 ng/mL), norgestrel (2 nM), β-estradiol (1 nM) and dexamethasone (31.6 nM). Compound effects are shown as log2-transformed fold change.

batch were normalized to their respective MLPmin sensor cell line controls (HEK293 assays to MLPmin from HEK293 control batch, PC12 assays to MLPmin from PC12 control batch, T-47D assays to MLPmin from T-47D control batch) for each biological replicate and condition. This normalization controlled for technical variables such as cell number and transfection efficiency while retaining cell-intrinsic effects like signaling pathway expression [28]. Internal barcode replicates (three for receptors, one for pathways) were averaged to represent one biological replicate. For luciferase assays, raw firefly luminescence values were used. Biological replicates were averaged, and standard errors were calculated. These averages and errors were then normalized for curve fitting, ranging from 0 % to 100 % for agonist dose-response assays. For antagonist treatments and co-culturing medium tests, the lowest compound concentration and the regular culturing medium were set to 100 %, respectively. Dose-response curves were visualized using the *drc* package in R. Assay robustness was evaluated using the Z′ factor (see section on statistical analysis), with results for potent inhibitors listed in Table S5. For heatmaps, log2 transformed fold changes were plotted, with the smallest compound concentration set to 0. In the luciferase test of stimuli pool and barcoded viability assays, the control group was set to 1. All plots were generated using the *ggplot2* package in R.

2.10.2. Statistical analysis

The robustness of dose-response assays was assessed using the Z′ factor, which considers both the means and standard deviations of high and low values [29]. The Z′ factor is calculated using the formula: $Z' = 1 - (3(SDH + SDL) / |meanH - meanL|)$, where SDH and SDL are the standard deviations of the high and low values, and meanH and meanL are the averages of the high and low values. A Z′ value of 0.5 or above indicates a robust assay. Statistics for the effect of PC12 medium on assays developed in HEK293 and T-47D cells was calculated using the *rstatix* package, while for CCK-8 assays the *emmeans* package was combined with the *rstatix* package. Significance for both assays was determined using one-way ANOVA with the Benjamini-Hochberg post hoc test. The significance of fold changes in luciferase reporter assays and the barcoded cell viability assay where only two samples were compared was calculated using a *t*-test with the *ggpubr* package. Barcoded assays were conducted in triplicates, luciferase reporter and CCK-8 assays in six replicates, and live cell luciferase assays in duplicates.

3. Results

3.1. Design of a barcoded assay for the safety profiling of compounds on GPCRs, RTKs, nuclear receptors and protease targets and their signaling activities

To establish a multiplex assay that measures the efficacy and side effects of compounds on targets and physiological pathways, we selected four GPCRs (ADRA1A, AVPR1A, DRD2, HTR2A); Fig. S1A), two RTKs (EGFR, ERBB4); Fig. S1B), three nuclear receptors (Ar, ESR1, GR); Fig. S1C), and one protease (BACE1); Fig S1D) as key drug target classes to be included in the barcoded profiling assay, termed safetyProfiler (Fig. 1, step 1, Table 1).

The selection of cell lines was guided by assay performance, with human cells, particularly HEK293, prioritized whenever feasible. However, for assays measuring the activity of GPCR targets such as ADRA1A, AVPR1A, and HTR2A, rat PC12 cells demonstrated superior performance compared to U2OS cells, another human cell line. Assays conducted in PC12 cells exhibited a higher signal-to-noise ratio, fold change, and overall robustness, which justified their selection [18]. Likewise, EGFR and ERBB4 assays showed a robust assay performance with higher fold changes in PC12 cells when compared to HEK293 cells or U2OS cells (Fig. S2A-B). Therefore, we selected PC12 cells for these five targets. However, when using rat-derived PC12 cells in pharmacological screens, the user is advised to control for potentially active drug metabolites on drug efficacy, as rat cells are known to exhibit a rather high level of xenobiotic metabolism [30].

Table 1
Targets and assays used in the safetyProfiler assay. Split TEV assays directly measure target activity. Pathways assays include MAPK, cAMP, and calcium signaling.

Target class	Receptor	Cell line	Type of assays
GPCR	ADRA1A	PC12	Split TEV, pathway
GPCR	AVPR1A	PC12	Split TEV, pathway
GPCR	DRD2	HEK293	Split TEV, pathway
GPCR	HTR2A	PC12	Split TEV, pathway
RTK	EGFR	PC12	Split TEV, pathway
RTK	ERBB4	PC12	Split TEV, pathway
Nuclear receptor	Ar	T−47D	NR element, pathway
Nuclear receptor	ESR1	HEK293	NR element, pathway
Nuclear receptor	GR (NR3C1)	HEK293	NR element, pathway
Protease	BACE1	HEK293	Cleavage assay on Nrg1-GV, pathway

The activity of each target was monitored directly at the site of action and at a pathway level to assess downstream physiological effects using genetically encoded reporter assays (Fig. 1, step 2). The activation of GPCRs and RTKs at the membrane was measured using the split TEV protein-protein interaction assay technique [31]. The split TEV assay is based on the protein-protein interaction induced functional complementation of two previously inactive TEVp fragments. The NTEV fragment, the TEVp cleavage site (tcs), and the artificial transcriptional co-activator GV were fused to the C-terminus of a GPCR or an RTK (see plasmids used in Fig. S1B, C, and Table S1). As interacting protein, a truncated version of β-arrestin-2 (residues 1–383 of ARRB2) was fused to CTEV to yield ARRB2–1–383-CTEV (Fig. S1E) for GPCR split TEV recruitment assays to monitor ligand guided activation of ADRA1A, AVPR1, DRD2, HTR2A. Similarly, the three times clustered SH2 domain of GRB2 fused to CTEV to yield 3xSH2(GRB2)-CTEV (Fig. S1F), which was applied in RTK split TEV recruitment assays to measure the activation of EGFR and ERBB4. Both of these adapters, ARRB2–1–383-CTEV and 3xSH2(GRB2)-CTEV, interact stimulus-dependent with GPCRs or RTKs, respectively. TEVp proteolytic activity liberates the membrane-trapped GV to induce barcode and firefly reporter gene transcription via the 10xUAS reporter. The activity of nuclear receptors was monitored by the cognate receptor response elements each linked to a unique barcode and firefly luciferase reporter as a readout (AR-RE, ER-RE, GR-RE; Fig. S1G). Consequently, the ligand induced translocation of a nuclear receptor to the nucleus activated the transcription of the reporter. The protease activity of BACE1, a membrane-spanning protein, was measured through the release of GV, which was fused to the C-terminus of neuregulin 1 (Nrg1-GV; Fig. S1H). Nrg1 is also a transmembrane protein and one of the targets of BACE1, thus serving as substrate for BACE1 in this assay [25,32]. As in the split TEV assays, protease-released GV translocated to the nucleus and bound to the 10xUAS reporter to activate transcription of the barcode and luciferase reporters (Fig S1I) to capture assay activity. The cellular responses of target activation were assessed for each target using a set of pathway sensors that responded to cAMP signaling, calcium signaling, and mitogen-activated protein kinase (MAPK) signaling (Fig. S1J). While cAMP signaling was measured with the CRE reporter (also measures calcium signaling), pure calcium signaling was captured using the NFAT-RE reporter. MAPK signaling was monitored using the EGR1p reporter, which specifically monitors the MAPK activity of the ERK1/2 branch [26]. Accordingly, the safetyProfiler assay yielded a total of 40 assays for the ten selected targets, comprising a simultaneous measurement of an activity assay and three pathway assays.

In this safetyProfiler assay, cellular batches each expressing one target, were pooled and plated together in a single well to conduct multiple assays in parallel (Fig. 1, step 3). To accomplish this, assay cells

were separately transfected with plasmids encoding each target and unique barcode reporters for measuring both the direct activity of receptors and their regulated downstream pathways. In addition, a constitutively active minimal major late promoter (MLPmin) was co-transfected to control batches of cells. Each treatment was applied in triplicate, while all compounds were administered in eight concentrations at a logarithmic scale (Fig. 1, step 4). Next, cells were lysed, well barcodes were added to lysates to process 24 samples in one (Tag&Pool, see Material and Methods). Barcode reporters were extracted from lysates, amplified by two rounds of PCRs, and sequenced using NGS (Fig. 1, step 5) [18,20]. Multiplexing of barcodes was performed at three levels. First, barcodes expressed from sensors are first level barcodes. Second, wells were tagged by well barcodes with a second level barcode. And third, amplification PCRs were using third level barcodes to enable further multiplexing of samples. Finally, barcode frequency was quantitatively analysed by calibrating them to the internal constitutive control promoter MLPmin of the control batch, normalized to the unstimulated control (agonist assays) or the lowest inhibitor concentration (antagonist assays), and visualized (Fig. 1, step 6).

3.2. *Establishment of optimal experimental conditions for the parallelized measurement of disease-relevant target activities and pathways*

A key aspect in the development of multiplexed assays for various targets, particularly for those belonging to different target classes, is the identification of a suitable time point for analysis following a ligand-induced stimulation. This is required to enable robust measurement of activity across all included targets, which can then be used in a multiplexed assay. Therefore, we monitored the activity of each target in a live cell assay using luminescence as a readout. Initially, we conducted continuous live cell tests for previously established GPCR and RTK split TEV assays [18,21]. Following ligand stimulation, the peak activities were observed at 9 h for ADRA1A; 6 h for AVPR1A, HTR2A and EGFR; 10 h for DRD2; and 14 h for ERBB4, thereby confirming our previous data (Fig. 2A–F). Next, it was key to establish experimental parameters for protein families previously not tested in a profiler setting, i.e., nuclear receptors and a protease target. We assessed whether nuclear receptor elements responded to their ligands without overexpressing the nuclear receptor itself (Fig. S2C-E). For AR-RE and GR-RE, we observed a robust response. For ER-RE, however, no response was observed when HEK293 cells were treated with β-estradiol, supporting the notion that ESR1 must be co-expressed to yield a response. Moreover, using the approach of overexpressing nuclear receptors enabled us to capture any changes in signaling downstream of a strongly activated receptor, as observed when overexpressing ERBB4 in PC12 cells and sensitizing the ERK1/2 signaling response to EGF-like domain (EGFld) [26]. Therefore, we tested whether co-expressing nuclear receptors together with their respective response elements generated robust assays, as all tested nuclear receptors responded to their respective stimuli (Fig. 2G–I). The peak activity for Ar, ESR1, and GR was observed at approximately 14 h, 26 h, and 11 h, respectively. Then, we produced dose-response data for these nuclear receptor assays at their peak time points (Fig. S2F-H). All the assays showed high affinity to their respective ligands, with EC_{50} values in the nanomolar range for Ar and GR, and reaching even a picomolar value for ESR1. Upon integrating the robustness and peak performance of all stimulation-based assays tested, it was determined that the time point at twelve hours following stimulation exhibited a reasonable measurement window. Earlier time points would have excluded the ESR1 assay, whereas later time points would have excluded AVPR1A and HTR2A assays. Accordingly, the duration of the cell culture phase of the assay was 48–52 h, depending on the length of starvation (Fig. S2I). The BACE1 assay is the only assay that was conducted as a constitutive assay, as protease activity is readily present when the CMV promoter-driven BACE1 cDNA was constitutively expressed from the transfected plasmid. The assay showed a stronger response in HEK293 cells persisting approximately 20 h (Fig. 2J) compared to PC12 cells in which it lasted approximately 1 h only (Fig. S2J). It peaked in activity at 44 h and at 20 h after transfection in HEK293 and PC12 cells, respectively. Due to the late peak and long duration of protease activity in HEK293 cells, it was possible to integrate the BACE1 assay with stimulation assays.

Assays for which the establishment has been described above, were conducted in three different cell lines, namely HEK293, PC12, and T-47D cells. In a barcoded profiling assay, it was necessary to co-culture these in the same well using a medium that all three cell lines can grow in. Since the largest number of assays was developed in PC12 cells (5 assays, see Table 1), we decided to test whether assays conducted in HEK293 and T-47D cells were also functional using PC12 medium. Therefore, HEK293 and T-47D cells transfected with the plasmids encoding the components of their respective assays (see Table 1) were plated in either their regular plating condition (i.e., T-47D medium for T-47D cells, HEK293 medium for HEK293 cells), in a 50:50 mixture of the regular plating medium and PC12 medium, or in PC12 medium only. Notably, changing the medium showed no significant effect in any of the tested assays, justifying the use of PC12 medium for co-cultured multiplexed assays (Fig. 2K). To monitor the growth performance of each cell line in a live cell assay, each cell line was transfected with a unique and constitutively expressed fluorescent protein as marker (EBFP2 into HEK293 cells, EGFP into PC12 cells, and mCherry into T-47D cells), pooled and plated into one well. The culturing of cells in the safetyProfiler assay was conducted for a period of 48–52 h. Therefore, we needed to ensure that optimal cell culture conditions were maintained for aa minimum of 52 h. Cells were co-cultured for 96 h and imaged at 24-hour intervals (Fig. S2K). At each time point imaged, all three cell lines displayed a normal morphology in the co-culture, including at the critical 48-hour time point (Fig. 2L).

3.3. *Activating receptors from various target classes using a pool of stimuli reflects the combined activation pattern of single agonist treatments*

In pharmacological assays, it is essential to have a measurement window, defined as Z' factor, that allows capturing either activating or inhibitory effects [29]. While agonistic effects on receptors can be monitored in assays simply by adding ligands, effects of antagonists are measured in co-treatment assays where receptors are simultaneously stimulated to an EC_{80} value using their cognate agonists, such as dopamine stimulating dopamine receptors and serotonin stimulating serotonin receptors, and so on. To reduce the number of wells and hence expenses and hands-on-time in multiplex assays, ligands can be pooled for all tested receptors, rather than stimulating each receptor individually. To address this, we conducted barcoded dose-response assays both with single stimuli and an agonist pool. In the single ligand agonist assays, GPCR ligands selectively stimulated GPCRs but promiscuity existed for GPCR ligands among GPCR targets. At the target level, GPCR agonists dopamine and epinephrin activated their cognate targets DRD2 and ADRA1A at the low micromolar range and showed promiscuity for activating the other receptor, which is consistent with our previous data [18] and findings from others [19]. Serotonin activated HTR2A at the nanomolar range and exhibited an even broader promiscuity, as, in addition to HTR2A, ADRA1A, AVPR1A, and DRD2 were activated. By contrast, vasopressin treatment led to the selective activation of AVPR1A only, exhibiting a high affinity for its receptor at the low nanomolar range. We confirmed dose-responses and EC_{50} values of previously developed GPCR assays (Table S6, Fig. 3A) [18,26]. At the pathway level, cAMP/calcium, pure calcium, and MAPK sensors were activated downstream of ADRA1A, AVPR1A, and HTR2A, while MAPK signaling was unaffected downstream of DRD2. Epinephrine treatment led to the strongest activation of cAMP/calcium signaling downstream of ADRA1A among all assays tested. Notably, dopamine and serotonin treatment also led to the activation of cAMP and calcium signaling downstream of ADRA1A, supporting the notion of ligand promiscuity. By contrast, ligands for RTKs and nuclear receptors selectively

stimulated their cognate targets only, without exhibiting promiscuity. For EGFR and ERBB4, the two RTKs of the profiling assay, we confirmed the selective and dose-dependent activation by EGF and EGFld, respectively. Furthermore, we were able to validate the agonist effect of EGF and EGFld on the ERK branch of MAPK signaling, which is captured by the MAPK sensor EGR1p [26]. Notably, EGF treatment led to the potent activation of MAPK signaling in EGFR and, to a lesser degree, in other target assays as well as in control assays that did not ectopically express any target (Fig. S3A). This repeated pattern of signaling behavior is due to the strong endogenous expression of EGFR in PC12 cells, as stimulated EGFR is known to activate the ERK branch of MAPK signaling [33]. For the newly developed nuclear receptor assays, EC_{50} values obtained from the barcoded assays were comparable to the ones obtained in standard luciferase assays, which served as benchmarking assays (Fig. S3B-D). The BACE1 protease assay showed no response to any other tested ligand. Treating the assay cells with the pooled ligands (see Table S7 for concentrations applied) produced results for each target assay that were highly similar to those obtained when using single ligands (compare far right column with pooled ligands to other columns in Fig. 3A, Fig. S3). In addition, we noticed that the agonist pool showed some toxicity when ligands were applied at the highest concentration. Dopamine exhibited some toxicity at single treatments as well, as PC12 and HEK293 cells treated with high concentrations of dopamine exhibited reduced receptor and pathways activity (e.g., for dopamine at 31 μM and 100 μM). A cellular stress response is indicated by activation of the CRE response in PC12 cells (e.g., for epinephrin at 31 μM and 100 μM, and norgestrel at 100 μM) (Fig. S3A) [26,34,35]. To solve this toxicity issue in the antagonist assays, where all ligands were administered as pool, we reduced the concentrations of the ligands to the lowest concentration that was shown to robustly activate GPCRs in cell based assays (1 μM for all targets) [18] and applying the nuclear receptor agonists in a low nanomolar range (Table S7). Before a barcoded compound profiling assay was conducted, the efficacy of the agonist pool with the adjusted ligand concentrations was tested on all receptors individually using single luciferase assays (Fig. 3B). Fold changes of stimulation were similar to the barcoded assay and ranged from approximately 2.5 (Ar, EGFR, ESR1) to 25 (HTR2A, GR), with most of the assays in a range of approximately 10–15-fold. Importantly, reducing the concentration of the single ligands in the agonist pool abolished any toxicity. This fine-tuning of the ligands in the agonist pool enabled us to use effective concentrations of each ligand and to reduce the total well number by the factor of nine due to co-administration of ligands in antagonist assays.

In its presented format, the profiling assay comprised ten targets and three pathways per target, totaling 40 data points per well. Per target, we used three barcode reporters for 10xUAS sensors assessing target activities and one barcode reporter for pathway sensors. In addition, three control batches of the sensors and included barcoded baseline controls, the overall amount of 81 barcodes were sequenced per well. Due to the complexity of the barcodes, the requirement to obtain a robust read count for each sensor in each well, and the transfection-based method that was chosen to genetically manipulate the assay cells, 71,000 cells (13,500 HEK293 cells; 5500 T-47D cells; 52,000 PC12 cells) were required and cultured in a single well of a 48-well plate (see Methods). Accordingly, sensors with low read counts of less than 150 under baseline conditions were excluded from further analysis.

3.4. *Barcoded profiling using the safetyProfiler assay reveals known and previously uncharacterized properties of approved drugs*

Next, we endeavored to challenge the barcoded safetyProfiler assay to generate profiles of selected drugs and tool compounds that target receptors that are present in this assay. Therefore, we selected drugs that target GPCRs (i.e., clozapine, paliperidone, risperidone, and the tool compound LE300), RTKs (i.e., pyrotinib and the failed drug AG1478 [36]), nuclear receptors (i.e., bazedoxifene, elacestrant, LY2452473, relacorilant, mifepristone, and spironolactone), and BACE1 (i.e., BACE1inhibitor IV and DAPT). In addition, we included canrenone, a metabolite of spironolactone; nocodazole, an anti-mitotic agent targeting microtubules; and staurosporine, a broad-band kinase inhibitor. In total, we profiled 17 drugs with eight increasing concentrations on ten targets, with four assays per target and three replicates per condition, yielding 16,320 data points collected for this profiling assay (Fig. 4).

The ERBB family antagonists AG1478 and pyrotinib inhibited both ligand-stimulated EGFR and ERBB4, albeit with mutual reverse preferences. While AG1478 preferentially inhibited EGFR over ERBB4 on both the receptor level and in MAPK signaling, pyrotinib displayed the reverse pattern, with a preferential inhibition of ERBB4 and downstream MAPK signaling. These findings for AG1478 and pyrotinib are consistent with our recent study, thus validating the principle and sensitivity of this safetyProfiler assay (Fig. 4) [26]. In addition, AG1478 and pyrotinib showed some promiscuity to GPCRs. AG1478 reduced both HTR2A and DRD2 activity as well as MAPK signaling downstream of these two GPCRs, and to a lesser extent, it was similar for ADRA1A and AVPR1A. Higher concentrations of AG1478 also inhibited calcium signaling downstream of DRD2 and HTR2A. By contrast, pyrotinib only caused a substantial inhibition on HTR2A and HTR2A-mediated MAPK2 signaling. Both effects can be explained through HTR2A's interaction with EGFR signaling [37]. The inhibitory effect on MAPK signaling downstream of ADRA1A and AVPR1A observed for pyrotinib can be explained by pyrotinib's effect on PC12 cells alone, as pyrotinib inhibited MAPK signaling downstream of endogenous EGFR in these cells (see condition baseline PC12, Fig. 4).

The atypical antipsychotic clozapine inhibited its renown targets DRD2 and HTR2A as well as calcium signaling downstream of these two receptors. The CRE sensor also responded to clozapine treatment, as this sensor element also captures calcium signaling [26]. Furthermore, clozapine also inhibited, although to a lesser degree, AVPR1A as well as calcium signaling. Notably, MAPK signaling was inhibited only downstream of HTR2A, but neither downstream of DRD2 nor of ADRA1A, suggesting a receptor-selective antagonism of MAPK signaling for clozapine. The antipsychotic risperidone, and its metabolite paliperidone, also inhibited ADRA1A, DRD2, HTR2A, and all signaling pathways measured. Interestingly, the efficacy of both risperidone and paliperidone for ADRA1A was higher compared to clozapine (Fig. 5A–C). Furthermore, risperidone and paliperidone, unlike clozapine, inhibited MAPK signaling downstream of all three GPCRs, while clozapine antagonized MAPK signaling only downstream of HTR2A (Fig. 5D–F). The tool compound LE300 displayed a similar profile like clozapine, with a high affinity to HTR2A and DRD2, and a rather mild inhibition of ADRA1A (Fig. 5G). ADRA1A activity antagonized by LE300 and paliperidone was quantified for the first time. In addition, the downstream signaling profile for LE300 resembled clozapine's profile, as cAMP and calcium signaling was largely antagonized, while MAPK signaling was not (Fig. 5H). LE300, paliperidone and risperidone regulated MAPK, cAMP, and calcium signaling downstream of ADRA1A, DRD2, and HTR2A was quantified for the first time as well.

The nuclear receptor inhibitors bazedoxifene, elacestrant, LY2452473, and relacorilant were selective for their receptors, i.e., bazedoxifene and elacestrant inhibited ESR1, LY2452473 inhibited Ar, and relacorilant inhibited GR (Fig. 4). Using this safetyProfiler assay, we were the first to determine an IC_{50} value for LY2452473 on Ar (8.565 nM) (Fig. 5I). By contrast, mifepristone displayed promiscuity among nuclear receptors and antagonized both Ar and GR. Spironolactone inhibited Ar and, when applied at higher concentrations, also antagonized activities of GR, ERBB4, ADRA1A, AVPR1A, and HTR2A. The inhibition of ERBB4 and HTR2A by spironolactone is in agreement with our previous studies [26,38]. Canrenone, a metabolite of spironolactone, showed no inhibition of any target, except for mild inhibition of Ar and GR when applied at higher concentrations. Interestingly, bazedoxifene was the only nuclear receptor inhibitor to show an effect on downstream signaling, as MAPK signaling was antagonized

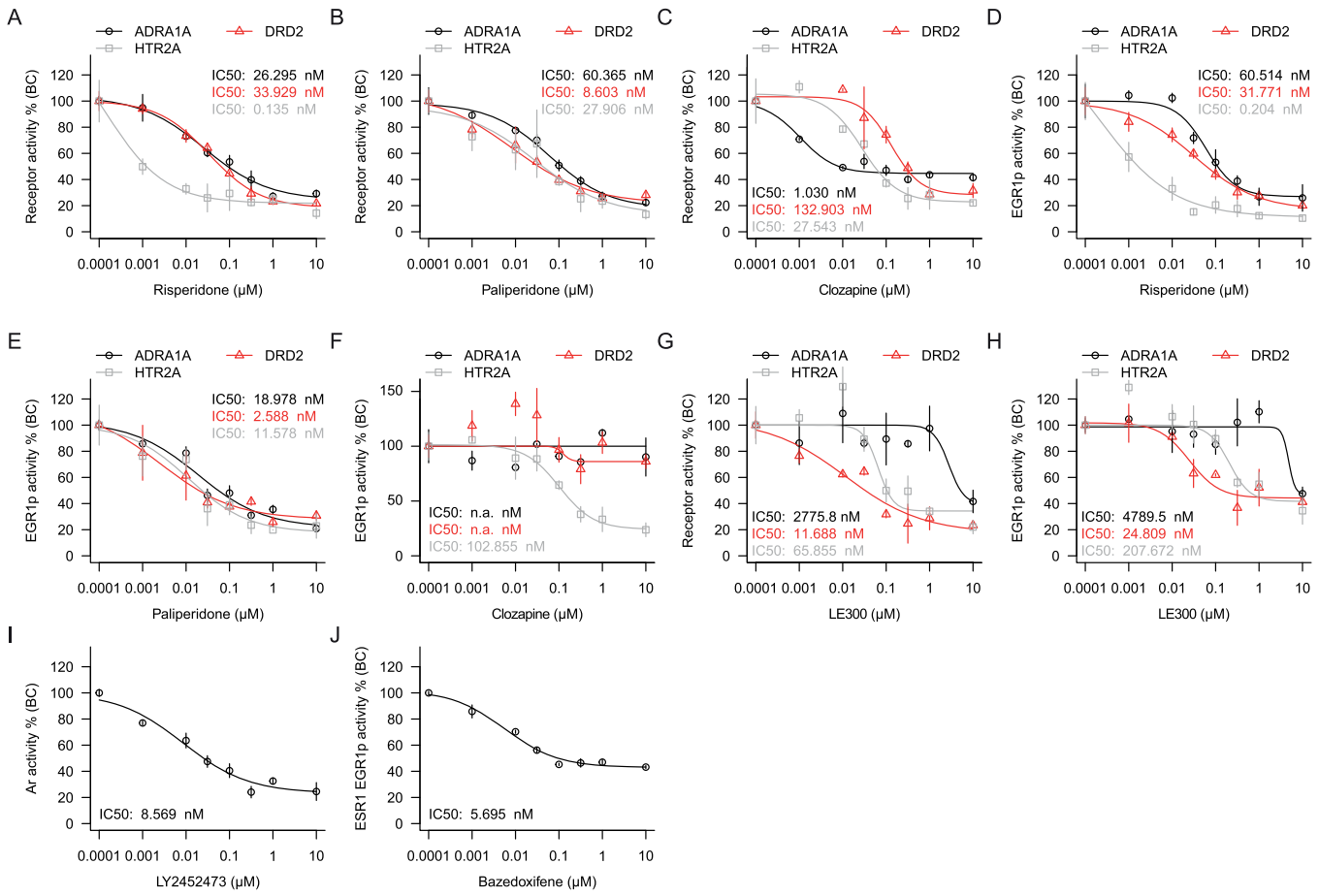

Fig. 5. The polypharmacology of neuroleptics demonstrates a promiscuous targeting profile and the capacity to discriminate in the inhibition of MAPK signaling. (A–C) Dose response assays displaying drug selectivity for (A) risperidone, (B) paliperidone, and (C) clozapine on ADRA1A, DRD2, and HTR2A. Activity of the GPCRs was measured using barcoded split TEV assays. (D-F) Dose response assays displaying drug selectivity for (D) risperidone, (E) paliperidone, and (F) clozapine on MAPK signaling measured downstream of ADRA1A, DRD2, and HTR2A. MAPK activity was measured by the barcoded EGR1p reporter. (D) Dose-response assay showing the inhibition of Ar by LY2452473. Activity was measured by AR-RE reporter. E) Dose-response assay showing the inhibition of MAPK signaling downstream of ESR1 by bazedoxifene. Data was extracted from the heatmap shown in Fig. 4. Error bars represent SEM, n = 3.

by bazedoxifene, with an IC_{50} of 5.695 nM (Fig. 5J) [39]. Elacestrant exhibited toxicity to all three cell lines at 10 μM (Fig. 4 and S4A), which was independently validated using a CCK-8 viability assay (Fig. S4A, B).

The administration of BACE1 inhibitor IV and DAPT resulted in a reduction of BACE1 activity, with DAPT also exerting a modest effect on downstream MAPK signaling. Finally, we tested nocodazole, a microtubule-depolymerizing drug, which had no direct effect on any of the receptors tested. In addition, staurosporine, a promiscuous kinase inhibitor, inhibited EGFR and ERBB4, while having a potent effect on all signaling pathways measured in all three cell lines. Specifically, staurosporine inhibited activities of EGFR, ERBB4, and MAPK signaling, while simultaneously activating calcium and cAMP signaling. The most pronounced activating effect of this compound was observed on the CRE sensor in PC12 cells (Fig. S4C), which was confirmed by a luciferase assay (Fig. S4D). Although not to the same extent as staurosporine, other drugs (e.g., bazedoxifene, LY2452473, and relacorilant) also activated cAMP signaling at high concentrations in PC12 cells, presumably due to cellular stress [26,34,35]. All IC_{50} values are summarized in Table S8.

4. Discussion

We present a cell-based multiplex profiling assay, termed safetyProfiler, which can simultaneously profile the efficacy, potency, and side effects of drugs to disease-relevant target molecules and cellular pathways through a multi-level barcoding approach. In particular, we have incorporated targets from diverse target classes and selected a panel of GPCR, RTKs, nuclear receptors, and a protease as targets in this assay enabling both the direct quantitative measurement of their activity and the simultaneous quantitative assessment of their impact on MAPK, cAMP, and calcium signaling. The readout for all assays used transcriptional barcode reporters that were driven by selective genetic sensors. These sensors either responded to the direct activation of the targets through GV release activated by split TEV for GPCRs and RTKs, or by BACE1/γ-secretase cleavage of Nrg1-GV as substrate (measured by a 10xUAS sensor), by activated nuclear receptors localized to the nucleus and binding to their cognate response elements (measured by AR-RE, ER-RE, and GR-RE sensors), or by MAPK signaling via ERK1/2 (measured by an EGR1p sensor), by cAMP and calcium signaling via CREB (measured by a CRE sensor), or by sole calcium signaling via NFAT (measured by an NFAT-RE sensor). Importantly, 40 different activity measurements for ten targets and three pathways per target were obtained from a single well. This comprehensive array of functional assays was assessed in the three distinct cell lines, namely HEK293, PC12, and T-47D cells, all of which were used to facilitate the functionality of a corresponding target assay. In particular, five assays were conducted in PC12 cells, four assays in HEK293 cells, and one assay in T-47D cells. As cell types were pooled and assay cells were stimulated in parallel and simultaneously lysed, we had to address two critical factors for the successful establishment of the safetyProfiler assay. First, it was necessary to select an appropriate duration of stimulation time ensuring that

all target assays exhibited a robust and sensitive response. Assays conducted in PC12 cells and T-47D cells showed a rather fast peak response compared to assays in HEK293 (note that the protease-assay was constitutive). Regarding stimulation time, the selected time point at 12 h post stimulation exhibited robust responses to increased concentrations of ligands for all targets tested. It is worth noting that administering nine single ligands as pool was toxic for cells at higher ligand concentrations. For the ten targets used in this study, this toxicity issue was solved by administering lower ligand concentrations that still resulted in efficient activation of each target. However, this could be a limiting factor when implementing more targets and thus pooling of a larger number of ligands may be required. A potential solution would be to divide the pool of stimuli into two sub-pools, which contain a limited number of ligands only. Second, it was essential to identify an appropriate medium for culturing and maintaining the viability of all three cell lines as well as preserving the functionality of each assay. We found that the PC12 cell medium was appropriate for the assays and cell types selected. This is, however, subject to change when either additional assays or cell types would be included into the multiplex assay. Furthermore, the implementation of stably expressed targets and lentivirus-delivered pathway reporters may facilitate an increase in barcode complexity per well, while simultaneously miniaturizing the vessel format. These stable human cell lines could therefore streamline the workflow for this multiplex assay as all cells in the culture will express targets and barcoded reporters, which should enable a more relevant and consistent assay, that is both sensitive and cost-effective for the profiling of drugs.

Using a single human cell line will also ensure a more uniform metabolic environment and enhance the assay's translatability to human biology. This is particularly important due to the well-established differences in drug metabolism between species [30]. These considerations align with recent guidance on drug metabolite safety testing, particularly the FDA's updated metabolites in safety testing (MIST) guidelines, which emphasize the importance of identifying and characterizing drug metabolites that, while non-toxic, may still impact the system, especially where disproportionate metabolites exist [40]. Drug metabolism occurs in three phases: Phase I modifies the drug through processes such as oxidation, reduction, hydrolysis, and cyclization/decyclization; Phase II conjugates it for inactivation and increased water solubility through reactions like methylation, acetylation, sulfation, glucuronidation, and glutathione conjugation; and Phase III excretes the conjugates, potentially involving further modification [41]. HEK293 cells exhibit minimal to undetectable Phase I xenobiotic-metabolizing enzymes (XMEs) [42], whereas rat PC12 cells are metabolically active and express a range of Phase I cytochrome P450 enzymes (CYP1A1, 1A2, 2B1, and 2E1) that respond rapidly to xenobiotics like monocrotophos, a widely used organophosphate pesticide [43]. The presence of these Phase I enzymes in rat cells leads to significant CYP induction within hours of exposure, resulting in the generation of reactive oxygen species (ROS), depletion of reduced glutathione, and upregulation of apoptotic proteins like caspase-3, caspase-9, and Bax. Interestingly, we also observed CRE activation, indicating cellular stress at high compound concentrations in PC12 cells, but not in human HEK293 or T-47D cells (see Fig. 4), potentially reflecting species-specific metabolic differences. Notably, the cytochrome P450 enzymes from PC12 cells can influence metabolic processes in HEK293 cells, potentially inactivating compounds and affecting their toxicity [44]. Additionally, both ROS and the apoptotic proteins may promote apoptosis in HEK293 cells [45]. While the primary role of XMEs is to detoxify and eliminate xenobiotics, certain compounds can also become activated during these processes, particularly in Phase I metabolism [40]. The differences in drug metabolism between species, particularly in Phase I with active cytochrome P450 enzymes in rat PC12 cells, but not in human HEK293 cells, underscore the potential for substantial alterations in drug-induced metabolic outcomes and toxicity, which may influence our assay results. Employing a normalization approach that controls for intrinsic cellular effects like CRE activation by using a cell line lacking the overexpressed target of interest, could partially resolve these discrepancies of the safetyProfiler assay in its current setup [28]. However, by transferring the assay platform to human cell lines would avoid the species-specific metabolites produced by rat-derived PC12 cells, including xenobiotic-metabolizing enzymes, which could otherwise influence assay outcomes [40,42–45].

The safetyProfiler assay was leveraged to assess the selectivity and potency of known drugs that antagonize clinically most relevant protein families, which are typically considered as a target panel when conducting safety profiling, including GPCRs, RTKs, nuclear receptors and a γ-secretase [46]. In addition, we included drugs that do not target any of the selected protein families (i.e., nocodazole as microtubule depolymerizing agent) or are known to be promiscuous and target multiple receptors within a protein family (i.e., staurosporine inhibiting nearly all RTKs and kinases in general) to assess the selectivity vs promiscuity. Notably, all drugs applied exhibited antagonism to their destined target. Moreover, drugs that showed promiscuity mostly targeted other receptors within the same protein family. For example, AG1478, an EGFR antagonist, also inhibited ERBB4, but displayed a clear preference for EGFR over ERBB4. Conversely, pyrotinib, designed as EGFR/ERBB2 antagonist, displayed a preference for ERBB4 over EGFR. Both findings were replicated in this dataset [26].

The three neuroleptics clozapine, paliperidone, and risperidone, as well as the tool compound LE300, exhibited potent inhibition of their respective GPCR targets and downstream pathways, but also promiscuity to other GPCRs. As in agreement with literature, all four drugs target DRD2 and HTR2A [47–49]. In addition, clozapine, paliperidone, and risperidone displayed promiscuity to the adrenergic receptor ADRA1A, but showed substantial differences in potency. While paliperidone and risperidone strongly inhibited ADRA1A, clozapine treatment only led to a mild inhibition of ADRA1A and downstream pathways. These fine-tuned differences in the polypharmacological profiles of neuroleptics are thought to contribute to the successful treatment of positive symptoms of schizophrenic patients [50].

The activity of nuclear receptors is tightly connected with multiple cancer types, as they play oncogenic and/or tumor-suppressive roles [51]. ESR1 and AR are the two nuclear receptors mostly targeted in clinical trials [52]. These two nuclear receptors are associated with reproductive cancers, but also play a role in other cancer types such as head, neck or lung cancer, hepatocellular carcinoma as well as in the control of tumor inflammation and immunity [51,53]. Nuclear receptors are known for their mutual crosstalk, which can be both cooperative and competitive [51]. One well studied cooperation is between AR and GR, where they regulate a common subset of genes and GR confers resistance to antiandrogens, especially in prostate cancer [54]. Conversely, GR expression in $ESR1^{+}$ breast cancer improves the treatment outcome [55], while its expression in $ESR1^{-}$ breast cancer is linked to a low survival rate [56]. Furthermore, in $ESR1^{+}$ endometrial cancer, GR co-expression is associated with poor prognosis [57], adding another layer of crosstalk complexity. In this study, we have profiled the effects of selected nuclear receptor antagonists that are currently tested in drug repurposing studies or were approved as single or multi-target drugs in the treatment of cancer. Mifepristone, a GR antagonist initially approved for abortion and now in phase 2 clinical drug repurposing trials for androgen cancers and phase 3 clinical drug repurposing trials for major depression, displayed a selective antagonistic profile for GR and AR. Bazedoxifene, an approved menopausal drug currently in phase 2 for breast cancer, and elacestrant, a recently approved drug against breast cancer [58] showed selectivity towards ESR1. Bazedoxifene's antagonistic effect was also observed in MAPK signaling. Elacestrant exhibited the highest toxicity at 10 μM of all compounds tested and in all cell lines used in our assay. Both LY2452473, an androgen inhibitor that has completed phase 2 trials for prostate cancer, and relacorilant, a glucocorticoid inhibitor currently in phase 2 for prostate cancer, as well as in phase 3 trials for Cushing's syndrome and for ovarian, peritoneal and

fallopian-tube cancer, showed highly selective profiles for their respective targets, thereby supporting the hypothesis that these drugs will likely receive market approval. Moreover, we were the first to measure an IC_{50} value for LY2452473, providing additional data that supports the potential for a phase 3 clinical trial for prostate cancer. We also confirmed the promiscuity of spironolactone, a steroid drug known for its off-target effects, not only among nuclear receptors (e.g., AR, GR, and mineralocorticoid receptor) [59–62], but also among other protein classes as well (e.g., ADRA1A, AVPR1A, HTR2A, and ERBB4) [26,38,60]. By integrating the safetyProfiler assay into the drug discovery pipeline, the selectivity profile of potentially promiscuous drugs, such as steroids, could be assessed faster and at reduced costs, thus accelerating drug development for complex diseases such as cancer and neuropsychiatric disorders. BACE1 drugs were initially designed as a potential treatment for Alzheimer's disease. However, due to the severe side effects on Notch signaling, the majority of the drugs did not progress to clinical trials or were discontinued prematurely [63,64]. In our assay, DAPT and BACE1 inhibitor IV showed a selective inhibitory effect on BACE1. However, it would be intriguing to examine their impact on Notch signaling in future studies. Many drugs activated the CRE sensor in PC12 cells at higher concentrations (e.g., pyrotinib, risperidone, bazedoxifene, LY2452473, relacorilant, canrenone, and nocodazole), with staurosporine having the strongest effect even at smaller concentrations. Notably, CRE sensor activation by staurosporine was observed in HEK293 and T-47D cells as well. Since pure calcium signaling, as measured by the NFAT-RE sensor was not upregulated, and CRE can respond to both cAMP and calcium signaling cues, this indicates that cellular stress occurred due to upregulated cAMP signaling, as we have demonstrated before [26].

5. Conclusion

We have developed a cell-based barcoded profiling assay which integrates diverse disease-relevant target classes, including GPCRs, RTKs, nuclear receptors, a protease, and key cellular pathways to evaluate the selectivity and potency of drugs, as well as potential off target effects. Using a readout of dynamically expressed barcodes from target and pathway sensors, the activity of ten targets and three major signaling pathways were measured in parallel to establish the polypharmacological profiles of 17 drugs, for some of which we identified novel properties. Taken together, this multiplexed safetyProfiler assay could pave the way for more informed drug development by providing highly informative polypharmacological drug profiles, thereby reducing the rate of drug attrition.

CRediT authorship contribution statement

Michael C. Wehr: Writing – review & editing, Writing – original draft, Visualization, Supervision, Resources, Project administration, Investigation, Funding acquisition, Formal analysis, Data curation, Conceptualization. **Moritz J. Rossner:** Writing – review & editing, Resources, Investigation, Funding acquisition, Conceptualization. **Giulia Palladino:** Writing – review & editing, Methodology. **Ben Brankatschk:** Writing – review & editing, Methodology, Investigation. **Lukša Popović:** Writing – review & editing, Writing – original draft, Visualization, Validation, Software, Investigation, Formal analysis, Data curation.

Consent for publication

All authors read and approved the manuscript.

Declaration of Competing Interest

The authors declare competing financial interest. B.B., M.J.R., and M.C.W. are employees and shareholders of Systasy Bioscience GmbH.

Data and resources availability

Data of barcoded safetyProfiler assays and orthogonal validation assays have been deposited at Mendeley Data (10.17632/tbb34fsj9w.1) and is publicly available as of the date of publication.

The original code has been deposited at Mendeley Data (doi: 10.17632/tbb34fsj9w.1) and is publicly available as of the date of publication.

Plasmids are available from Addgene.

Supporting Information

Supplementary data associated with this article can be found in the online version.

Declaration of Competing Interest

The authors declare the following financial interests/personal relationships which may be considered as potential competing interests: Michael Wehr reports financial support was provided by Ludwig Maximilians University LMU University Hospital Munich. Luksa Popovic reports financial support was provided by Systasy Bioscience GmbH. Ben Brankatschk reports financial support was provided by Systasy Bioscience GmbH. Giulia Palladino reports financial support was provided by Systasy Bioscience GmbH. Moritz Rossner reports financial support was provided by Ludwig Maximilians University LMU University Hospital Munich. Michael Wehr reports a relationship with Systasy Bioscience GmbH that includes: employment and equity or stocks. Ben Brankatschk reports a relationship with Systasy Bioscience GmbH that includes: employment and equity or stocks. Moritz Rossner reports a relationship with Systasy Bioscience GmbH that includes: employment and equity or stocks. If there are other authors, they declare that they have no known competing financial interests or personal relationships that could have appeared to influence the work reported in this paper.

Data availability

Data of barcoded safetyProfiler assays and orthogonal validation assays have been deposited at Mendeley Data (10.17632/tbb34fsj9w.1) and is publicly available as of the date of publication.

Acknowledgements

We thank Barbara Meisel and Monika Rübekeil for excellent technical support. The research was supported by the Bayrische Forschungsstiftung, Munich, Germany, grant number AZ-1469-20, and by the European Union HORIZON-MSCA-2022-DN-01 funded IDPro doctoral network, grant agreement number 101119633.

Appendix A. Supporting information

Supplementary data associated with this article can be found in the online version at doi:10.1016/j.biopha.2024.117523.

References

[1] L.M. McNamee, M.J. Walsh, F.D. Ledley, Timelines of translational science: from technology initiation to FDA approval, PLoS One (2017), https://doi.org/10.1371/journal.pone.0177371.
[2] J. Zurdo, Developability assessment as an early de-risking tool for biopharmaceutical development, Pharm. Bioprocess. (2013), https://doi.org/10.4155/pbp.13.3.
[3] A. Gaulton, L.J. Bellis, A.P. Bento, J. Chambers, M. Davies, A. Hersey, Y. Light, S. McGlinchey, D. Michalovich, B. Al-Lazikani, et al., ChEMBL: a large-scale bioactivity database for drug discovery, Nucleic Acids Res. *40* (2012) D1100–D1107, https://doi.org/10.1093/nar/gkr777.
[4] J. Arrowsmith, Trial watch: Phase II failures: 2008-2010, Nat. Rev. Drug Discov. *10* (2011) 328–329, https://doi.org/10.1038/nrd3439.

[5] I.J. Onakpoya, C.J. Heneghan, J.K. Aronson, Post-marketing withdrawal of 462 medicinal products because of adverse drug reactions: a systematic review of the world literature, BMC Med. *14* (2016), https://doi.org/10.1186/s12916-016-0553-2.

[6] N.S. Craveiro, B.S. Lopes, L. Tomás, S.F. Almeida, Drug withdrawal due to safety: a review of the data supporting withdrawal decision, CDS *15* (2020) 4–12, https://doi.org/10.2174/1574886314666191004092520.

[7] A.K. Giri, A. Ianevski, T. Aittokallio, Genome-wide off-targets of drugs: risks and opportunities, Cell Biol. Toxicol. *35* (2019) 485–487, https://doi.org/10.1007/s10565-019-09491-7.

[8] M.J. Waring, J. Arrowsmith, A.R. Leach, P.D. Leeson, S. Mandrell, R.M. Owen, G. Pairaudeau, W.D. Pennie, S.D. Pickett, J. Wang, et al., An analysis of the attrition of drug candidates from four major pharmaceutical companies, Nat. Rev. Drug Discov. *14* (2015) 475–486, https://doi.org/10.1038/nrd4609.

[9] R.R. Ramsay, M.R. Popovic-Nikolic, K. Nikolic, E. Uliassi, M.L. Bolognesi, A perspective on multi-target drug discovery and design for complex diseases, Clin. Transl. Med *7* (2018), https://doi.org/10.1186/s40169-017-0181-2.

[10] O. Méndez-Lucio, J.J. Naveja, H. Vite-Caritino, F.D. Prieto-Martínez, J.L. Medina-Franco, O. Méndez-Lucio, J.J. Naveja, H. Vite-Caritino, F.D. Prieto-Martínez, J. L. Medina-Franco, Review. One drug for multiple targets: a computational perspective, J. Mex. Chem. Soc. *60* (2016) 168–181.

[11] Andrade, E.L., Bento, A.F., Cavalli, J., Oliveira, S.K., Freitas, C.S., Marcon, R., Schwanke, R.C., Siqueira, J.M., and Calixto, J.B. (2016). Non-clinical studies required for new drug development – Part I: Early in silico and in vitro studies,new target discovery and validation,proof of principles and robustness of animal studies. Preprint, https://doi.org/10.1590/1414-431X20165644 https://doi.org/10.1590/1414-431X20165644.

[12] Whitebread, S., Hamon, J., Bojanic, D., and Urban, L. (2005). Keynote review: In vitro safety pharmacology profiling: An essential tool for successful drug development. Preprint, https://doi.org/10.1016/S1359-6446(05)03632-9 https://doi.org/10.1016/S1359-6446(05)03632-9.

[13] Bowes, J., Brown, A.J., Hamon, J., Jarolimek, W., Sridhar, A., Waldron, G., and Whitebread, S. (2012). Reducing safety-related drug attrition: The use of in vitro pharmacological profiling. Preprint, https://doi.org/10.1038/nrd3845 https://doi.org/10.1038/nrd3845.

[14] Oprea, T.I., Bologa, C.G., Brunak, S., Campbell, A., Gan, G.N., Gaulton, A., Gomez, S.M., Guha, R., Hersey, A., Holmes, J., et al. (2018). Unexplored therapeutic opportunities in the human genome. Preprint, https://doi.org/10.1038/nrd.2018.14 https://doi.org/10.1038/nrd.2018.14.

[15] A. Abbasi, L.B. Alexandrov, Significance and limitations of the use of next-generation sequencing technologies for detecting mutational signatures, DNA Repair *107* (2021) 103200, https://doi.org/10.1016/j.dnarep.2021.103200.

[16] K. Lohmann, C. Klein, Next generation sequencing and the future of genetic diagnosis, Neurotherapeutics *11* (2014) 699–707, https://doi.org/10.1007/s13311-014-0288-8.

[17] C. Cheng, Z. Fei, P. Xiao, Methods to improve the accuracy of next-generation sequencing, Front. Bioeng. Biotechnol. *11* (2023) 982111, https://doi.org/10.3389/fbioe.2023.982111.

[18] S. Galinski, S.P. Wichert, M.J. Rossner, M.C. Wehr, Multiplexed profiling of GPCR activities by combining split TEV assays and EXT-based barcoded readouts, Sci. Rep. (2018), https://doi.org/10.1038/s41598-018-26401-9.

[19] H. Chen, C.E. Rosen, J.A. González-Hernández, D. Song, J. Potempa, A.M. Ring, N. W. Palm, Highly multiplexed bioactivity screening reveals human and microbiota metabolome-GPCRome interactions, Cell *186* (2023) 3095–3110.e19, https://doi.org/10.1016/j.cell.2023.05.024.

[20] E.M. Jones, R. Jajoo, D. Cancilla, N.B. Lubock, J. Wang, M. Satyadi, R. Cheung, C. de March, J.S. Bloom, H. Matsunami, et al., A Scalable, Multiplexed assay for decoding GPCR-ligand interactions with RNA sequencing, Cell Syst. *8* (2019) 254–260.e6, https://doi.org/10.1016/j.cels.2019.02.009.

[21] J.P. Wintgens, S.P. Wichert, L. Popovic, M.J. Rossner, M.C. Wehr, Correction to: Monitoring activities of receptor tyrosine kinases using a universal adapter in genetically encoded split TEV assays, Cell. Mol. Life Sci. 76 (6) (2019) 1185–1199, 10.1007/s00018-018-03003-2). Preprint, https://doi.org/10.1007/s00018-019-03244-9 https://doi.org/10.1007/s00018-019-03244-9.

[22] A. Herholt, V.K. Sahoo, L. Popovic, M.C. Wehr, M.J. Rossner, Dissecting intercellular and intracellular signaling networks with barcoded genetic tools, Curr. Opin. Chem. Biol. *66* (2022) 102091, https://doi.org/10.1016/j.cbpa.2021.09.002.

[23] Y. Wu, N. Jensen, M.J. Rossner, M.C. Wehr, Exploiting cell-based assays to accelerate drug development for G protein-coupled receptors, IJMS *25* (2024) 5474, https://doi.org/10.3390/ijms25105474.

[24] V. Blay, B. Tolani, S.P. Ho, M.R. Arkin, High-throughput screening: today's biochemical and cell-based approaches, Drug Discov. Today *25* (2020) 1807–1821, https://doi.org/10.1016/j.drudis.2020.07.024.

[25] D. Fleck, M. Voss, B. Brankatschk, C. Giudici, H. Hampel, B. Schwenk, D. Edbauer, A. Fukumori, H. Steiner, E. Kremmer, et al., Proteolytic processing of neuregulin 1 type III by three intramembrane-cleaving proteases, J. Biol. Chem. (2016), https://doi.org/10.1074/jbc.M115.697995.

[26] L. Popović, J.P. Wintgens, Y. Wu, B. Brankatschk, S. Menninger, C. Degenhart, N. Jensen, S.P. Wichert, B. Klebl, M.J. Rossner, et al., Profiling of ERBB receptors and downstream pathways reveals selectivity and hidden properties of ERBB4 antagonists, iScience *27* (2024) 108839, https://doi.org/10.1016/j.isci.2024.108839.

[27] A. Herholt, B. Brankatschk, N. Kannaiyan, S. Papiol, S.P. Wichert, M.C. Wehr, M. J. Rossner, Pathway sensor-based functional genomics screening identifies modulators of neuronal activity, Sci. Rep. (2018), https://doi.org/10.1038/s41598-018-36008-9.

[28] L. Popović, M.J. Rossner, M.C. Wehr, Protocol for identifying properties of ERBB receptor antagonists using the barcoded ERBBprofiler assay, STAR Protoc. *5* (2024) 102987, https://doi.org/10.1016/j.xpro.2024.102987.

[29] Chung Zhang, Oldenburg, A simple statistical parameter for use in evaluation and validation of high throughput screening assays, J. Biomol. Screen *4* (1999) 67–73.

[30] M. Martignoni, G.M.M. Groothuis, R. de Kanter, Species differences between mouse, rat, dog, monkey and human CYP-mediated drug metabolism, inhibition and induction, Expert Opin. Drug Metab. Toxicol. *2* (2006) 875–894, https://doi.org/10.1517/17425255.2.6.875.

[31] M.C. Wehr, R. Laage, U. Bolz, T.M. Fischer, S. Grünewald, S. Scheek, A. Bach, K.-A. Nave, M.J. Rossner, Monitoring regulated protein-protein interactions using split TEV, Nat. Methods *3* (2006) 985–993, https://doi.org/10.1038/nmeth967.

[32] M. Willem, A.N. Garratt, B. Novak, M. Citron, S. Kaufmann, A. Rittger, B. DeStrooper, P. Saftig, C. Birchmeier, C. Haass, Control of peripheral nerve myelination by the beta-secretase BACE1, Science *314* (2006) 664–666, https://doi.org/10.1126/science.1132341.

[33] S. Kao, R.K. Jaiswal, W. Kolch, G.E. Landreth, Identification of the mechanisms regulating the differential activation of the mapk cascade by epidermal growth factor and nerve growth factor in PC12 cells, J. Biol. Chem. *276* (2001) 18169–18177, https://doi.org/10.1074/jbc.M008870200.

[34] M. Aslam, Y. Ladilov, Emerging role of cAMP/AMPK signaling, Cells *11* (2022) 308, https://doi.org/10.3390/cells11020308.

[35] P. Tanzarella, A. Ferretta, S.N. Barile, M. Ancona, D. De Rasmo, A. Signorile, S. Papa, N. Capitanio, C. Pacelli, T. Cocco, Increased levels of cAMP by the calcium-dependent activation of soluble adenylyl cyclase in parkin-mutant fibroblasts, Cells *8* (2019) 250, https://doi.org/10.3390/cells8030250.

[36] W.B. Weglicki, J.H. Kramer, C.F. Spurney, J.J. Chmielinska, I.T. Mak, The EGFR tyrosine kinase inhibitor tyrphostin AG-1478 causes hypomagnesemia and cardiac dysfunction, Can. J. Physiol. Pharmacol. *90* (2012) 1145–1149, https://doi.org/10.1139/y2012-023.

[37] M. Göőz, P. Göőz, L.M. Luttrell, J.R. Raymond, 5-HT2A receptor induces ERK phosphorylation and proliferation through ADAM-17 tumor necrosis factor-alpha-converting enzyme (TACE) activation and heparin-bound epidermal growth factor-like growth factor (HB-EGF) shedding in mesangial cells, J. Biol. Chem. *281* (2006) 21004–21012, https://doi.org/10.1074/jbc.M512096200.

[38] M.C. Wehr, W. Hinrichs, M.M. Brzózka, T. Unterbarnscheidt, A. Herholt, J. P. Wintgens, S. Papiol, M.C. Soto-Bernardini, M. Kravchenko, M. Zhang, et al., Spironolactone is an antagonist of NRG1-ERBB4 signaling and schizophrenia-relevant endophenotypes in mice, EMBO Mol. Med. (2017), https://doi.org/10.15252/emmm.201707691.

[39] T. Jover-Mengual, M. Castelló-Ruiz, M.C. Burguete, M. Jorques, M.A. López-Morales, A. Aliena-Valero, A. Jurado-Rodríguez, S. Pérez, J.M. Centeno, F. J. Miranda, et al., Molecular mechanisms mediating the neuroprotective role of the selective estrogen receptor modulator, bazedoxifene, in acute ischemic stroke: a comparative study with 17β-estradiol, J. Steroid Biochem. Mol. Biol. *171* (2017) 296–304, https://doi.org/10.1016/j.jsbmb.2017.05.001.

[40] J. Shanu-Wilson, L. Evans, S. Wrigley, J. Steele, J. Atherton, J. Boer, Biotransformation: impact and application of metabolism in drug discovery, ACS Med. Chem. Lett. *11* (2020) 2087–2107, https://doi.org/10.1021/acsmedchemlett.0c00202.

[41] O.A. Almazroo, M.K. Miah, R. Venkataramanan, Drug metabolism in the liver, Clin. Liver Dis. *21* (2017) 1–20, https://doi.org/10.1016/j.cld.2016.08.001.

[42] W. Qu, D.M. Crizer, M.J. DeVito, S. Waidyanatha, M. Xia, K. Houck, S.S. Ferguson, Exploration of xenobiotic metabolism within cell lines used for Tox21 chemical screening, Toxicol. Vitr. *73* (2021) 105109, https://doi.org/10.1016/j.tiv.2021.105109.

[43] M.P. Kashyap, A.K. Singh, V. Kumar, V.K. Tripathi, R.K. Srivastava, M. Agrawal, V. K. Khanna, S. Yadav, S.K. Jain, A.B. Pant, Monocrotophos Induced Apoptosis in PC12 Cells: role of xenobiotic metabolizing cytochrome P450s, PLoS One *6* (2011) e17757, https://doi.org/10.1371/journal.pone.0017757.

[44] M. Kumondai, E. Hishinuma, E.M. Gutiérrez Rico, A. Ito, Y. Nakanishi, D. Saigusa, N. Hirasawa, M. Hiratsuka, Heterologous expression of high-activity cytochrome P450 in mammalian cells, Sci. Rep. *10* (2020) 14193, https://doi.org/10.1038/s41598-020-71035-5.

[45] D. Liu, Y. Wang, S. Ma, H. Sun, W. Shi, X. Feng, Individual and combined use of ginsenoside F2 and cyanidin-3-O-glucoside attenuates H_2O_2-induced apoptosis in HEK-293 cells via the NF-κB pathway, RSC Adv. *7* (2017) 41713–41722, https://doi.org/10.1039/C7RA04689H.

[46] T. Papoian, H.-J. Chiu, I. Elayan, G. Jagadeesh, I. Khan, A.A. Laniyonu, C.X. Li, M. Saulnier, N. Simpson, B. Yang, Secondary pharmacology data to assess potential off-target activity of new drugs: a regulatory perspective, Nat. Rev. Drug Discov. *14* (2015), https://doi.org/10.1038/nrd3845-c1, 294–294.

[47] H. Xiamuxi, Z. Wang, J. Li, Y. Wang, C. Wu, F. Yang, X. Jiang, Y. Liu, Q. Zhao, W. Chen, et al., Synthesis and biological investigation of tetrahydropyridopyrimidinone derivatives as potential multireceptor atypical antipsychotics, Bioorg. Med. Chem. *25* (2017) 4904–4916, https://doi.org/10.1016/j.bmc.2017.07.040.

[48] M. Kondej, P. Stępnicki, A.A. Kaczor, Multi-target approach for drug discovery against schizophrenia, Int. J. Mol. Sci. *19* (2018) 3105, https://doi.org/10.3390/ijms19103105.

[49] M. Decker, K.-J. Schleifer, M. Nieger, J. Lehmann, Dopamine/serotonin receptor ligands. Part VIII[1]:the dopamine receptor antagonist LE300 - modelled and X-ray structure plus further pharmacological characterization, including serotonin

receptor binding, biogenic amine transporter testing and in vivo testings, Eur. J. Med. Chem. *39* (2004) 481–489, https://doi.org/10.1016/j.ejmech.2004.02.001.
[50] M. Lähteenvuo, J. Tiihonen, Antipsychotic polypharmacy for the management of schizophrenia: evidence and recommendations, Drugs *81* (2021) 1273–1284, https://doi.org/10.1007/s40265-021-01556-4.
[51] V.K. Dhiman, M.J. Bolt, K.P. White, Nuclear receptors in cancer - uncovering new and evolving roles through genomic analysis, Nat. Rev. Genet. (2018), https://doi.org/10.1038/nrg.2017.102.
[52] Z. Yang, R.C. Gimple, N. Zhou, L. Zhao, J.-Å. Gustafsson, S. Zhou, Targeting nuclear receptors for cancer therapy: premises, promises, and challenges, Trends Cancer *7* (2021) 541–556, https://doi.org/10.1016/j.trecan.2020.11.007.
[53] L. Zhao, H. Hu, J.-Å. Gustafsson, S. Zhou, Nuclear receptors in cancer inflammation and immunity, Trends Immunol. *41* (2020) 172–185, https://doi.org/10.1016/j.it.2019.12.006.
[54] V.K. Arora, E. Schenkein, R. Murali, S.K. Subudhi, J. Wongvipat, M.D. Balbas, N. Shah, L. Cai, E. Efstathiou, C. Logothetis, et al., Glucocorticoid receptor confers resistance to antiandrogens by bypassing androgen receptor blockade, Cell *155* (2013) 1309–1322, https://doi.org/10.1016/j.cell.2013.11.012.
[55] D.C. West, D. Pan, E.Y. Tonsing-Carter, K.M. Hernandez, C.F. Pierce, S.C. Styke, K. R. Bowie, T.I. Garcia, M. Kocherginsky, S.D. Conzen, GR and ER coactivation alters the expression of differentiation genes and associates with improved ER+ breast cancer outcome, Mol. Cancer Res. *14* (2016) 707–719, https://doi.org/10.1158/1541-7786.MCR-15-0433.
[56] D. Pan, M. Kocherginsky, S.D. Conzen, Activation of the glucocorticoid receptor is associated with poor prognosis in estrogen receptor-negative breast cancer, Cancer Res. *71* (2011) 6360–6370, https://doi.org/10.1158/0008-5472.CAN-11-0362.
[57] J.M. Vahrenkamp, C.-H. Yang, A.C. Rodriguez, A. Almomen, K.C. Berrett, A. N. Trujillo, K.P. Guillen, B.E. Welm, E.A. Jarboe, M.M. Janat-Amsbury, et al., Clinical and genomic crosstalk between glucocorticoid receptor and estrogen receptor α in endometrial cancer, Cell Rep. *22* (2018) 2995–3005, https://doi.org/10.1016/j.celrep.2018.02.076.
[58] S.M. Hoy, Correction: elacestrant: first approval, Drugs *83* (2023), https://doi.org/10.1007/s40265-023-01978-2, 1735–1735.
[59] M. Lainscak, F. Pelliccia, G. Rosano, C. Vitale, M. Schiariti, C. Greco, G. Speziale, C. Gaudio, Safety profile of mineralocorticoid receptor antagonists: spironolactone and eplerenone, Int. J. Cardiol. *200* (2015) 25–29, https://doi.org/10.1016/j.ijcard.2015.05.127.
[60] J.J. Sutherland, D. Yonchev, A. Fekete, L. Urban, A preclinical secondary pharmacology resource illuminates target-adverse drug reaction associations of marketed drugs, Nat. Commun. *14* (2023) 4323, https://doi.org/10.1038/s41467-023-40064-9.
[61] R.D. Gabbard, R.R. Hoopes, M.G. Kemp, Spironolactone and XPB: an old drug with a new molecular target, Biomolecules *10* (2020) 756, https://doi.org/10.3390/biom10050756.
[62] C. Yang, H.C. Shen, Z. Wu, H.D. Chu, J.M. Cox, J. Balsells, A. Crespo, P. Brown, B. Zamlynny, J. Wiltsie, et al., Discovery of novel oxazolidinedione derivatives as potent and selective mineralocorticoid receptor antagonists, Bioorg. Med. Chem. Lett. *23* (2013) 4388–4392, https://doi.org/10.1016/j.bmcl.2013.05.077.
[63] S. Boopathi, A.B. Poma, R. Garduño-Juárez, An overview of several inhibitors for Alzheimer's disease: characterization and failure, IJMS *22* (2021) 10798, https://doi.org/10.3390/ijms221910798.
[64] J.-Y. Hur, γ-Secretase in Alzheimer's disease, Exp. Mol. Med. *54* (2022) 433–446, https://doi.org/10.1038/s12276-022-00754-8.